

The Decay of Debris Disks around Solar-Type Stars

J. M. Sierchio^{1,2}, G. H. Rieke¹, K. Y. L. Su¹, & Andras Gáspár¹

sierchio@mit.edu

ABSTRACT

We present a *Spitzer* MIPS study of the decay of debris disk excesses at 24 and 70 μm for 255 stars of types F4 - K2. We have used multiple tests, including consistency between chromospheric and X-ray activity and placement on the HR diagram, to assign accurate stellar ages. Within this spectral type range, at 24 μm , $13.6 \pm 2.8\%$ of the stars younger than 5 Gyr have excesses at the 3σ level or more, while none of the older stars do, confirming previous work. At 70 μm , $22.5 \pm 3.6\%$ of the younger stars have excesses at $\geq 3\sigma$ significance, while only $4.7^{+3.7}_{-2.2}\%$ of the older stars do. To characterize the far infrared behavior of debris disks more robustly, we double the sample by including stars from the DEBRIS and DUNES surveys. For the F4 - K4 stars in this combined sample, there is only a weak (statistically not significant) trend in the incidence of far infrared excess with spectral type (detected fractions of $21.9^{+4.8}_{-4.3}\%$, late F; $16.5^{+3.9}_{-3.3}\%$, G; and $16.9^{+6.3}_{-5.0}\%$, early K). Taking this spectral type range together, there is a significant decline between 3 and 4.5 Gyr in the incidence of excesses with fractional luminosities just under 10^{-5} . There is an indication that the timescale for decay of infrared excesses varies roughly inversely with the fractional luminosity. This behavior is consistent with theoretical expectations for passive evolution. However, more excesses are detected around the oldest stars than is expected from passive evolution, suggesting that there is late-phase dynamical activity around these stars.

Subject headings: circumstellar matter — infrared: stars — planetary systems: formation

¹ Steward Observatory, University of Arizona, Tucson, AZ 85721

² Currently at Department of Physics, Massachusetts Institute of Technology, Cambridge, Massachusetts 02139, USA

1. Introduction

Understanding planetary system formation and evolution is one of the major initiatives in astronomy. Stars form surrounded by protoplanetary disks of primordial gas and dust where planets grow. The material in these disks that does not fall into the star either collects into planets or is dissipated by processes such as photo-evaporation (e.g., Clarke et al. 2001) and tidal forces from planets (e.g., Bryden et al. 1999), typically in less than 10 Myr (Williams & Cieza 2011). The evolution of the systems is not complete, as shown by the events that led to the formation of our Moon and to the Late Heavy Bombardment (Tera et al. 1974), long after the protoplanetary disk cleared from the Sun. It is very difficult to observe these later stages of evolution directly. However, after dissipation of the protoplanetary disks, a relatively low level of dust production can be sustained through debris produced in planetesimal collisions to form planetary debris disks (Wyatt 2008), which can be detected readily in the infrared over the entire range of stellar lifetime (to 10 Gyr). Debris disks are our best current means of studying planet system evolution over its entire duration.

About 20% of the nearby stars harbor debris disks above current detection limits (Habing et al. 2001; Trilling et al. 2008; Carpenter et al. 2009; Gáspár et al. 2013; Eiroa et al. 2013). The likelihood of a detectable debris disk at 24 μm depends on age, with a higher percentage around young stars than older ones (e.g., Habing et al. 1999; Rieke et al. 2005; Gáspár et al. 2013). The expected timescale for evolution of the disk components that dominate in the far infrared indicates that, depending on disk location and density, there might also be a detectable decay in disk incidence at 70 μm (Wyatt 2008). However, it has proven difficult to confirm this prediction definitively (Wyatt 2008; Bryden et al. 2006; Trilling et al. 2008; Carpenter et al. 2009). Gáspár et al. (2013) have recently demonstrated a drop in infrared excess on the basis of comparison with the predictions of a theoretical model. If such a decay can be confirmed by an alternative analysis, it would help substantially to constrain models and particle properties of debris disks.

In this paper, we explore debris disk evolution in the far infrared (70 - 100 μm) using a large sample of stars to allow reaching statistically robust conclusions. The paper presents high-quality homogeneous data reductions for a large sample of stars observed with *Spitzer*, analyzes their behavior, and then combines this sample with the *Herschel*-observed DEBRIS (Mathews et al. 2010) and DUNES (Eiroa et al. 2013) samples. We take care in determining stellar ages, since the apparent rate of decay can be strongly influenced by mis-classification of the ages (a small number of young stars mistakenly identified as old ones might dominate the detections among the "old" sample). Section 2 describes the selection of the *Spitzer* sample, the determination of stellar ages, and the reduction of the infrared

measurements. We determined debris-disk-emitted excesses as described in Section 3. Section 4 presents the analysis of the behavior of these excesses with stellar age, and Section 5 merges this sample and additional *Spitzer* data with *Herschel* observations to study debris disk evolution in a total sample of about 470 stars. Our conclusions are summarized in Section 6.

2. Sample Selection and Data Reduction

2.1. Selection Criteria

2.1.1. Photometric Criteria

We used specific criteria to draw samples of stars from the entire *Spitzer* Debris Disk Database. All stars were required to have Hipparcos data (van Leeuwen 2007), with parallax errors not to exceed 10% (the smallest parallax in the sample is 10.7 mas). V magnitudes were taken from Hipparcos, transformed to Johnson V (Harmanec 1998). In general the sample is limited to stars with $24\ \mu\text{m}$ magnitudes less than 7 (i.e., to be brighter than ~ 12 mJy); the largest V magnitude is 8.59. All stars were also required to have observations on the 2MASS K_S system. These measurements were obtained from 2MASS when the measurement errors were indicated to be $< 3\%$. For stars with saturated measurements, K -band photometry from the literature was transformed to the 2MASS system, using relations in Carpenter (2001) or Koen et al. (2007) or derived for this study. A particularly important set of measurements is from the Johnson Bright Star program (Johnson et al. 1966a; Johnson 1966b), for which transformations are difficult to determine because of dynamic range issues (the faintest stars measured accurately in the infrared in the Bright Star program are too bright to be measured without saturation in 2MASS). In this case, we determined the transformation through intermediate steps to obtain:

$$K_S = K_{Johnson} - 0.0567 + 0.056(J - K)_{Johnson} \quad (1)$$

When at least three measurements had been made of a star in the Bright Star program (Johnson et al. 1966a), we found that the transformed result was within our 3% accuracy requirement, as judged by the scatter around standard colors. In the following discussion the V and K magnitudes will refer consistently to V magnitudes transformed to the Arizona (Johnson) system from Hipparcos measurements and to K_S magnitudes on the 2MASS system, either from 2MASS or transformed to that system.

Additional measurements were obtained at SAAO on the 0.75-m telescope using the

MarkII Infrared Photometer (transformed as described by Koen et al. (2007)), and at the Steward Observatory 61-Inch with a NICMOS2-based camera with a 2MASS filter set and a neutral density filter to avoid saturation. These measurements will be described in a forthcoming paper (Su et al. in preparation).

Our study is confined to solar-like stars, defined as having spectral types in the range of F4-K2 and of luminosity classes IV-V (obtained from SIMBAD). This places the Sun as G2 in the middle of our spectral type range. To guard against the uncertainties in spectral classifications, we used the photometric colors to select stars with $1.05 < V - K < 2.0$, which corresponds to the desired range of spectral types (Tokunaga 2000). The spectral types of the stars retained were consistent with their colors, although the color selection eliminated a few stars with indicated spectral types inside the desired range.

2.1.2. Other parameters

The original programs in which our sample stars were measured are identified in Table 1. A large majority (93%) come from seven *Spitzer* programs: 1.) the MIPS GTO sun-like star observations (Trilling et al. 2008); 2.) Formation and Evolution of Planetary Systems (FEPS) (Meyer et al. 2006); 3.) Completing the Census of Debris Disks (Koerner et al. 2010); 4.) potential SIM/TPF targets (Beichman et al. 2006); 5.) an unbiased sample of F-stars (Trilling et al. 2008); and 6.) two coordinated programs selecting stars on the basis of indicators of youth (Low et al. 2005; Plavchan et al. 2009). All of these programs were based on unbiased samples selected in differing ways. The remaining 7% of the sample come from a broad range of programs, but, with the single exception of HD 206893, none made selections on the basis of prior detections. Another source of bias is sources left off a selection because they are committed to guaranteed programs. This issue is most important for the MIPS solar type program, and Bryden et al. (2006) list four stars that would otherwise have been in their sample. Of them, HD 10647 is in our sample and HD 17206 is in the DEBRIS sample and will be included when we merge with it. HD 10700 (Chen et al. 2006) does not appear to have an excess at the wavelengths of interest (so it would have little influence on our results), while ϵ Eri is not in our sample. To first order, it and HD 206893 offset biases, since they are both young stars with substantial excesses. However, these details demonstrate that any sample compiled from a collection of other samples defined on different bases are subject to selection biases.

We checked SIMBAD and the literature for indications of stars being members of multiple star systems. Such stars were only allowed in the final sample if they had a separation of less than 1 arcsecond or greater than 12 arcseconds. For typical distances for the sample

members (≥ 8 pc), 12 arcsec corresponds to a separation ≥ 100 AU and hence avoids the possible bias against debris disks for binary separations less than this value (Trilling et al. 2007; Rodriguez & Zuckerman 2012). Close binaries were allowed because they do not appear to suppress outer debris disks (emitting in the far infrared) (Trilling et al. 2007). The original samples from which ours is drawn were not selected on the basis of rotational characteristics, although on the basis of gyrochronology we expect systematically higher *v_{sin}i* for the younger stars. After assembly of a preliminary sample, we carefully screened each star repeatedly for issues such as blending or complex backgrounds. The stars rejected in these tests were biased slightly toward being young but the distribution did not differ significantly from the age distribution of the entire sample (rejecting 10 in the 0 - 750 Myr range, 4 in 750 Myr - 5 Gyr, 4 in > 5 Gyr). Finally, we consider whether metallicity could bias our results, given the dependence of detected planets on metallicity (Fischer & Valenti 2005; Johnson et al. 2010). However, a number of studies imply that the dependence of debris-disk excesses on [Fe/H] is weak (Trilling et al. 2008; Maldonado et al. 2012), and that the correlation between the presence of planets and debris disks, although present, is also weak (Bryden et al. 2009; Maldonado et al. 2012). Any bias due to metallicity effects can also be discounted because the average [Fe/H] of the stars of ages < 5 Gyr is -0.13, whereas for those at ages > 5 Gyr, it is virtually identical at -0.15.

Given the requirements on spectral type and apparent magnitudes, the sample is almost entirely (95%) within 50 pc of the sun. The stars beyond this distance are representative of the sample as a whole: in average metallicity, [Fe/H] = -0.14; in average spectral type, F9V; in age, seven 0 - 700 Myr, three 700 Myr - 5 Gyr, three > 5 Gyr; and in incidence of excesses, 30%.

2.1.3. Ages

Accurately-measured ages are essential to determine the decay of debris excesses. If the excesses decay substantially over the age range of the sample of stars, a few young stars incorrectly classified as being old can seriously affect the apparent rate of decay. To ensure the accuracy of our results, we took a conservative approach by using three different methods to estimate ages: (1) placement on the HR-diagram, (2) chromospheric activity indices (CAI), and (3) X-ray luminosity. For the latter two indicators, we used the calibration of Mamajek & Hillenbrand (2008).

Each of these methods has weaknesses, making it desirable to use all three to verify the consistency of the results. Traditionally, use of the HR diagram can lead to relatively large errors in ages; the method is intrinsically inaccurate for stars near the main sequence, and it

can also give incorrect results for reasons such as undetected stellar multiplicity. However, used with care the HR diagram is useful for determining ages of stars old enough to have left the main sequence. In comparison, CAI ages are well-calibrated for stars older than ~ 300 Myr and younger than ~ 4 Gyr (Mamajek & Hillenbrand 2008). For stars younger than 300 Myr, the issues are complex and will be discussed below. For stars older than 4 Gyr, the calibration of Mamajek & Hillenbrand (2008) rests on only 23 stars with accurate ages from placement on the HR diagram. X-ray detections are also useful for young stars, but measurements of old stars are relatively uncommon. Because of their differing strengths and weaknesses, we tested the consistency of the indicators before proceeding with their use. For these tests, we drew stars from three samples studied extensively for debris disks: our combined *Spitzer* sample and those for the Herschel key programs DUNES and DEBRIS.

We compare the ages obtained via chromospheric activity with those from X-ray luminosity in Figure 1. The sources for the CAI, $\log R'_{HK}$, can be found in Table 2 and in Gáspár et al. (2013). X-ray detections were taken from the ROSAT data (Voges et al. 1999, 2000), with the requirement of positional matches within 30 arcsec and $-0.8 < \text{HR1} < 0$; this constraint on the hardness ratio (HR1) was adopted to avoid AGN ($\text{HR1} > 0.5$), stars that are possibly flaring ($0 < \text{HR1} < 0.5$) and background thermal sources ($\text{HR1} < -0.8$) (T. Fleming, private communication). The trend line in Figure 1 (fitted by linear least squares with equal weight for all points) has a nominal slope of 1.28 ± 0.05 , with a tendency for the points for the oldest stars to have larger ages from the CAI than from X-ray luminosity. This tendency could arise from a selection effect (Eddington bias). Only a minority of old stars are detected by ROSAT, and the limited ratios of signal to noise mean that the detected sample will tend to include stars slightly overestimated in X-ray flux (due to statistics), leading to underestimated ages.

We tested this possibility on the stars in our sample with ages ≥ 5 Gyr based on the CAI. We used the CAI age estimates, the parallaxes, and photometric data to predict the ROSAT count rate for each star, which we compared with the ROSAT data. We evaluated the detection limits for each star from typical measurements for faint sources in the ROSAT Faint Source Catalog (Voges et al. 2000) in a field of 1 degree radius around the star. These detection limits and the predicted counts for the star were used to calculate the probability that it would have been above the detection threshold (Voges et al. 2000) for the survey. The sum of these probabilities over the entire sample of stars was 18 and is an estimate of how many detections are expected if the CAI ages agree perfectly with those from X-ray emission. In fact, 27 stars could be identified with cataloged X-ray sources (Voges et al. 1999, 2000); however, three of them were so discordant from the count rate predictions for their ages and distances that the ROSAT detections are suspect and may arise from background sources. Therefore, we predict 18 detections and find 24, indicating that the X-ray fluxes

are slightly brighter than expected from the Mamajek and Hillenbrand (2008) calibration. However, at the 1σ level, virtually no correction is indicated; in addition X-ray emission and the CAI are measures of closely related stellar parameters. We therefore used the Mamajek and Hillenbrand (2008) calibration "as-is." Nonetheless, it would be desirable to test the X-ray age calibration against a larger sample of old stars.

We next used the *Spitzer*-DEBRIS-DUNES sample of stars (our sample plus those in Gáspár et al. (2013)) to compare CAI ages with those from the HR diagram. We select $V - K$ and M_K for the axes of the HR diagram, since the long wavelength baseline of $V - K$ makes it an accurate indicator of stellar temperature (Masana et al. 2006) and the K-band should be a relatively robust luminosity indicator, since it is in the Rayleigh-Jeans spectral regime for our sample of stars. To place the stars on the HR-diagram (Figure 2), we first eliminated from this expanded sample all cases with detected close companions (within $12''$) that would be included in or confuse the photometry of the star. The $V - K$ color is quite sensitive to metallicity (Li et al. 2007); M_V is also metallicity sensitive but this effect should be reduced for M_K given the simpler spectrum across the K window. To calibrate the effects of metallicity on the HR diagram, we determined a linear transformation that made the empirical metallicity-dependent isochrones of An et al. (2007) coincide over the range $-0.3 \leq [\text{Fe}/\text{H}] < 0.2$. We then reversed this transformation and applied it to each star so that stars of differing metallicity can be compared on a single HR diagram:

$$\textit{corrected } M_{K_S} = M_{K_S} + 0.5\left[\frac{\text{Fe}}{\text{H}}\right] \quad (2)$$

$$\textit{corrected } V - K_S = V - K_S - 0.25\left[\frac{\text{Fe}}{\text{H}}\right] \quad (3)$$

Metallicity measurements were obtained from a number of sources (e.g., Marsakov & Shevelev 1995; Gray et al. 2003; Valenti & Fischer 2005; Gray et al. 2006; Ammons et al. 2006; Holmberg et al. 2009; Soubiran et al. 2010); when more than one measurement was available, they were averaged. Stars with $[\text{Fe}/\text{H}] < -0.4$ were eliminated in this comparison (but not in our final study if we had reliable age indicators) because our metallicity correction is not calibrated for them. We used the isochrones from the Padua group for the final comparisons (Bonatto et al. 2004; Marigo et al. 2008), because they have better coverage for older stars than those of An et al. (2007). An empirical correction of -0.14 magnitudes was made to the absolute K_S magnitude on the isochrones to match the measured values for the main sequence; this correction removes systematic issues in matching the observational and theoretical photometric systems.

The majority of stars with ages indicated from the CAI greater than 6 Gyr fall between the 6 and 11 Gyr isochrones, as shown in Figure 2. Figure 3 compares the ages; a few stars

were eliminated from the sample based on this comparison because their ages from the HR diagram were much younger than from the CAI. Since it is difficult for binarity or other issues to produce such discrepancies, the CAI ages for these stars are suspect. There are 38 stars in the sample in Figure 3 older than 4 Gyr; the trend line (fitted by linear least squares with equal weight for all points) has a slope of 0.985 ± 0.027 , insignificantly different from 1, and there is no apparent deviation from the trend line with increasing age. We confirm that the CAI/X-ray calibration of Mamajek & Hillenbrand (2008) is consistent with isochrone ages for stars older than 4 Gyr.

With this validation, we have used chromospheric activity and X-ray luminosity as our primary age indicators. We supplemented these indicators with $\log g < 4$, which for stars over the relevant spectral range (F4 - K2) shows that a star is above the main sequence, and with gyrochronology ages when available. We then checked that the age was consistent with the placement of the star on the HR diagram. Stars where the initial criteria indicated ages > 5 Gyr, but which fell in an inappropriate region on the HR diagram, were not used further. The final *Spitzer* sample is presented in Table 2 with the V and K_S measurements, ages, and Spitzer measurements at $24 \mu\text{m}$ and $70 \mu\text{m}$. The age distribution of the sample is shown in Figure 4; there are 255 stars with age estimates, of which 238 have useful $70 \mu\text{m}$ measurements.

We now discuss the uncertainties in the ages. Taking ages directly from Mamajek & Hillenbrand (2008) would be circular, since we use the same calibration and some of the same data sources. However, comparing with those ages is revealing; there is a scatter of 0.15 dex. These differences primarily arise because of data published since the publication of Mamajek & Hillenbrand (2008), and they illustrate that there can be significant uncertainties despite the care we have taken in estimating stellar ages. Another issue is that there is a large spread in chromospheric activity around 50 - 300 Myr (Mamajek & Hillenbrand 2008). As a result, a star with a low level of activity may still be within this age range. Based on Figure 5 of Mamajek & Hillenbrand (2008), it is possible that about 20% of the stars in the 50 - 300 Myr range are incorrectly placed in the 0.6 - 2.5 Gyr one if the age is assigned purely on the basis of the CAI. This rate of incorrect age assignment is an upper limit because we use multiple indicators to check against each other. More importantly, we find that the incidence of debris disk excesses does not vary rapidly across the 0.1 - 2.5 Gyr age range (see Section 5.2), so a modest number of age errors within this range will have little effect on our results.

2.2. Data Reduction

2.2.1. 24 μm

We re-processed all the mid- and far-infrared data for these stars as part of a *Spitzer* legacy catalog, using the MIPS instrument team Data Analysis Tool (Gordon et al. 2005) for the initial reduction steps. In addition, a second flat field constructed from the 24 μm data itself was applied to all the 24 μm results to remove scattered-light gradients and dark latency (Engelbracht et al. 2007). The processed data were then combined using the World Coordinate System information to produce final mosaics with pixels half the size of the physical pixel scale (which is 2.49"). We extracted the photometry using point-spread function (PSF) fitting. The input PSFs were constructed using isolated calibration stars and have been tested to ensure that the photometry results are consistent with the MIPS calibration (Engelbracht et al. 2007). Aperture photometry was also performed, but the results were only used as a reference to screen targets that might have contamination from nearby sources or background nebulosity.

The random photometry errors were estimated based on the pixel-to-pixel variation within a 2 arcmin square box centered on the source position. The measured flux densities (using 7.17 Jy as the zero magnitude flux; (Rieke et al. 2008)), and associated random errors are listed in Table 2. The errors from the photometry repeatability ($\sim 1\%$ at 24 μm ; Engelbracht et al. (2007)) are included, which were measured on stars of similar brightness to our sample members (and hence give an estimate of photon noise as well as other systematic photometric errors). For the stars with indicated 24 μm excesses, we have compared with the WISE W3 - W4 color. In all cases where the WISE W4 measurement had adequate signal-to-noise, the MIPS measurement was confirmed¹. At least two of the stars in our sample have strong excesses at 24 μm and weak ones at 70 μm , placing them in the rare category of predominantly warm debris disks (HD 1466, for which the weak far infrared excess is confirmed with Herschel (Donaldson et al. 2012) and HD 13246 (Moor et al. 2009)).

2.2.2. 70 μm

The 70 μm observations were obtained in the default pixel scale (9.85"). After initial reprocessing, artifacts were removed from the individual 70 μm exposures as described in Gordon et al. (2007). The exposures were then combined with pixels half the size of the

¹The WISE data for HD 25457 show multiple sources and appear to be confused; the MIPS data are valid.

physical pixel scale. The image of each source was examined to be sure that it was free of confusing objects such as IR cirrus emission or background sources. A number of objects were rejected at this stage. PSF photometry was used to extract flux measurements for the ‘clean’ sources, utilizing STinyTim PSFs that had been smoothed to match the observations (accounting primarily for the effects of the pixel sampling) and with the position fixed to that found at 24 μm . The results were calibrated as in Gordon et al. (2007). The random photometry errors were based on pixel-to-pixel variations in a 2 arcmin field surrounding the source and are tabulated (including a 5% allowance for photometric non-repeatability (Gordon et al. 2007)) along with the flux densities in Table 2.

3. Determination of Excesses

3.1. 24 μm Excesses

Excesses at 24 μm were detected by using a V-K vs. K-[24] plot (Figure 5). The locus of stars without excesses was determined from a total of ~ 1320 stars drawn from the *Spitzer* archive, reduced identically to the stars in our sample, and with K-magnitudes from the same sources. The resulting fit is (Urban et al. 2012):

$$K_S - [24] = 0.0055 - 0.0134x + 0.06555x^2 - 0.1095x^3 + 0.066415x^4 - 0.01458x^5 + 0.001101x^6 - 0.000003x^7 \quad (4)$$

for $x > 0$ where x is $V - K_S - 0.8$. The scatter around this fit was determined for all 1320 stars by fitting a Gaussian to the residuals. Because a significant number of stars have excesses, the fitting parameters need to be selected to avoid a bias. We first used outlier rejection based on Huber’s Psi Function, set just to avoid rejecting any points below the photospheric value. We used the Anderson-Darling (A-D) test to confirm that the remaining distribution around the photospheric values was consistent with a normal distribution. Inspection of the results indicated that there were a number of stars with excesses (the positive side of the distribution above 0.03 in residual had 127 stars compared with 96 for the negative side of the distribution below -0.03), so before calculating the A-D p-value, we replaced the measures above 0.03 with the inverse of the ones below -0.03. The A-D test then indicated that the distribution around the photospheric value was indistinguishable from a Gaussian ($p = 0.14$). We therefore fitted a Gaussian to these points, finding a standard deviation of 0.0304.

To provide a more intuitive check of this approach, we carried out a second analysis where we fitted a Gaussian excluding values more than $2\text{-}\sigma$ above the photospheric trend line (that is above 0.06). As with use of the Psi Function, this strategy makes the fit independent of infrared excesses detected in some of the stars of the sample but is more

subjective than the outlier rejection approach. A demonstration of this result can be found in Ballering et al. (2013), which demonstrates the excellent fit of a Gaussian around the photospheric value as well as showing the population of excesses. In the current case, this Gaussian indicated a standard deviation of 0.0295. That is, the two Gaussian fits to the peak of the measurement distribution around the photospheric value agree closely in width. We adopt a value of $\sigma = 0.03$. Therefore, any star with a $K_S - [24] > 0.09$ magnitudes larger than predicted for its photosphere is considered to have an excess at 24 μm (nominally, the number of false identifications in our sample is then expected to be less than 0.5). None of the stars older than 1000 Myr have excesses based on this requirement; 23 of the younger stars do, a fraction of 0.136 ± 0.028 (errors from binomial statistics). Stars with excesses are listed in Table 3.

3.2. 70 μm Excesses

A method similar to that described in Trilling et al. (2008) was used to determine which stars had excesses at 70 μm . We computed an excess ratio, R^2 , for each star by predicting a photospheric flux density based on the measured flux density at 24 μm divided by 9.05 (the nominal ratio of flux densities between 24 and 70 μm) and then divided by the ratio of the measurement to the predicted photospheric value at 24 μm if this ratio exceeded one. We used the figure of merit:

$$\chi_{70} = (F_{70} - P_{70})/\sigma \quad (5)$$

to quantify the significance of an excess, where F_{70} is the measured flux density at 70 μm , P_{70} is the predicted photospheric flux density, and σ is the uncertainty in the flux density measurement at 70 μm (the uncertainty in P_{70} is negligible compared with that in F_{70} for our entire sample). In total 38 stars younger than 5 Gyr and 4 stars older than this age are considered to have excesses, as illustrated in Figure 6 and listed in Table 3. For the young sample, the probability of having an excess (at 70 μm) is $38/169 = 0.225 \pm 0.036$. Similarly for the old sample, the probability of an excess is $4/86 = 0.047_{-0.022}^{+0.037}$ (all errors are calculated from the "exact" or Clopper-Pearson method, based on binomial statistics). Three of the four detections around old stars are at $\chi_{70} > 4.5$ and should be very reliable (see Figure 6). These three systems are similar in amount of excess to typical younger stars; the ratios of the fluxes at 70 μm to the photospheric fluxes are close to the median for our entire sample.

²R is defined as the stellar flux density divided by that expected from the photosphere alone, $R = F_{70}/P_{70}$.

3.3. Stars Older Than 2.5 Gyr with 70 μm Excesses

The major conclusion from this paper will rest on the small number of old stars with excesses. The reliability of this number is influenced both by the reliability of the identification of excesses, and by the accuracy of our age estimates. With regard to the reliability of the excesses, we have compared with the results from the Herschel DUNES and DEBRIS surveys (as summarized in Gáspár et al. (2013) and Eiroa et al. (2013)). There are 50 stars in our sample also in the Herschel samples. Using the same $3\text{-}\sigma$ selection criterion, 41 of the 50 stars show no evidence for excess emission with either telescope³. Of the remaining nine stars, six show significant excesses in the data from both telescopes, (HD 20794, 30495, 33262, 76151, 199260, and 207129) and one more (HD 153597) has an excess close to 3σ in both sets of data. The remaining two stars are HD 30652, and 117176. The first case is just over the $3\text{-}\sigma$ threshold with PACS and at 1σ excess with MIPS (assuming 5% photometric errors plus the statistical errors); the two values agree within 1.8 standard deviations. However, the weighted average of the two measurements has a net excess at less than $3\text{-}\sigma$ significance, so we classify it as a non-excess star. For HD 117176, the MIPS measurement (at 70 μm) is right on the photospheric value while the PACS one (at 100 μm) is well above it; the two differ nominally by 4σ . The implied very cold spectral energy distribution for the excess suggests that it could arise from a background galaxy (Gáspár & Rieke 2014), so we have listed this star as not having an excess.

Because of the residual uncertainties in age, we will discuss the stars with excesses and with ages indicated to be greater than 2.5 Gyr (since we will show that the incidence of excesses drops substantially between 3 and 5 Gyr). At the same time we tabulate their spectral types to probe whether they are characteristic of the full sample. We begin with the stars indicated to have ages between 2.5 and 5 Gyr: *HD 20807*, G0V: The placement on the HR diagram indicates that this star is less than 3.5 Gyr old. As indicated in Table 1, multiple sources indicate chromospheric activity levels too high for the star to be 5 Gyr or older. *HD 33636*, G0V: The placement on the HR diagram indicates an age < 3.5 Gyr. Isaacson & Fischer (2010) report 17 measurements of chromospheric activity that are, with a single exception, consistent with the quoted age; the age should be robust against measurement errors and variations in activity. *HD 207129*, G2V: There are suggestions that we have overestimated the age of this star ((Montes et al. 2001; Mamajek & Hillenbrand 2008; Tetzlaff et al. 2011) but no indication that it could be older than 5 Gyr. We now

³HD 1237, 4308, 4614, 10307, 17051, 20630, 23754, 43162, 50692, 55575, 62613, 76943, 78366, 79028, 84737, 86728, 89269, 90839, 99491, 101501, 102365, 102438, 109358, 114710, 115383, 126053, 126660, 130948, 142860, 143761, 145675, 160691, 162003, 168151, 180161, 189245, 190422, 202275, 210277, 210302, and 212330

discuss the stars older than 5 Gyr and with 70 μm excesses: *HD 1461*, G0V: Two measurements (Wright et al. 2004; Gray et al. 2003) agree that the chromospheric activity of this star is very low, corresponding to an age of 7 to 8 Gyr. The placement on the HR diagram indicates a lower limit of 6 Gyr. *HD 20794*, G8V: Three measurements (Henry et al. 1996; Gray et al. 2006; Schröder et al. 2009) agree that this star has low chromospheric activity, indicating an age of ~ 7 Gyr. The position of the star on the HR diagram is inconclusive with regard to age. *HD 38529*, G4V: Multiple measurements (Wright et al. 2004; White et al. 2007; Schröder et al. 2009; Isaacson & Fischer 2010; Kasova & Livshits 2011) agree on the low chromospheric activity of this star, corresponding to an age of about 6 Gyr. The value of the CAI reported by Isaacson & Fischer (2010) is based on more than 100 measurements. The surface gravity also places this star well off the main sequence. *HD 114613*, G3-4 V: Four measurements (Henry et al. 1996; Jenkins et al. 2006; Gray et al. 2006; Isaacson & Fischer 2010) agree that this star has a very low level of chromospheric activity, corresponding to an age of about 8 Gyr. The value from Isaacson & Fischer (2010) is based on 28 individual measurements. The placement of the star on the HR diagram indicates an age > 5 Gyr; it also has low surface gravity, consistent with its position well above the main sequence.

4. Analysis

In this section, we first show that the rate of excess detection is independent of spectral type, confirming the result from Gáspár et al. (2013). As a result, to obtain good statistics, we can consider the evolution of the debris excesses combining the results for all spectral types without loss of information. We then analyze the time evolution of the excesses for the *Spitzer* sample. In the following section, we first show that the stars measured in the DEBRIS and DUNES programs behave consistently with the *Spitzer* sample and then combine all the data to double the number of stars. This larger sample shows that the incidence of far-infrared excesses evolves substantially with stellar age (see also Gáspár et al. (2013)).

4.1. Detection Statistics

Because our samples span late F-, G-, and early K- spectral types, we can report excess fractions for each type. To compute these fractions, we have consider only stars less than 5 Gyr old, since stellar evolution would otherwise be an issue for the F stars. Similarly, we consider only excesses at 70 μm , since the 24 μm excesses evolve over an age range of a Gyr. We find fractions with excesses of 16/63, 20/98, and 2/8 respectively for F4 - F9, G, and

K stars. We can combine our results with those from DEBRIS and DUNES (Gáspár et al. 2013; Eiroa et al. 2013), using the same definition for detection of an excess ($\chi > 3$). We have omitted HIP 171, 29271, and 49908 from this combined sample because their 160 μm excesses are likely to arise through confusion with background galaxies (Gáspár & Rieke 2014); we have also omitted HIP 40843, 82860, and 98959 because the reported excesses at 100 μm (Gáspár et al. 2013) may also be contaminated (Eiroa et al. 2013). The net results are 23/105, 22/133, and 10/69 respectively for F4 - F9, G, and K stars. The corresponding fractions are $0.219_{-0.043}^{+0.048}$, $0.165_{-0.033}^{+0.039}$, and $0.145_{-0.043}^{+0.055}$. If the ten stars later than K4 are excluded (all from the DEBRIS and DUNES samples and none of which have excesses), the fraction for K stars rises to $0.169_{-0.050}^{+0.063}$; the errors are 1σ , computed using the "exact" or Clopper-Pearson method, based on the binomial theorem. Although there may be a weak trend with spectral type, the incidence of excesses is (within the errors) the same for late F through early K-type stars. This conclusion is strengthened if we take account of the possible bias of including HD 206893 (F5V) and excluding ϵ Eri (K2V) in our sample, as discussed in Section 2.1.2. The results of previous studies are mixed, but our result is in general agreement with Trilling et al. (2008) who reported no clear trend of infrared excess detection with stellar type.

4.2. 70 μm Excess Evolution: K-M Test

Previous studies have attempted to quantify the decay rate for debris disks by one of two different approaches (Rieke et al. 2005; Trilling et al. 2008): counting the number of stars with detected excesses (i.e., basing the statistics on small excesses) or fitting the largest excesses (i.e., matching the apparent upper envelope of the excesses). Neither of these approaches takes rigorous account of all the data and each is subject to selection effects. In the first case, if the achieved sensitivity is not adequate to detect the stellar photospheres uniformly, the minimum detectable excess is not uniform, whereas in the second case the upper envelope of the excesses is ill-defined and based on small number statistics. Ultimately, these studies found either no or only weak evidence of disk evolution with age. The underlying problem can be described in terms of data censoring, that is, the non-uniform detection limits result in target stars being removed from the study at the levels of excess represented by upper limits.

A standard statistical approach to such a situation is to use the Kaplan-Meier (K-M) estimator, since it naturally allows for censored data (Feigelson & Babu 2012). We have used the version of the K-M estimator provided by Lowry (2013), which bases its confidence level estimates on the efficient-score method (Newcombe 1998). We divide the sample into

three equal parts corresponding to the age ranges < 750 Myr, $750 - 5000$ Myr, and > 5000 Myr. Based on the detection limits and identifications of excesses in Table 2, we find that the probable numbers of excess ratios $R > 1.5$ at $70 \mu\text{m}$ are 27% with 95% confidence limits of 18% and 38% for stars of age < 750 Myr and 22% with confidence limits of 14% and 33% for those between 750 and 5000 Myr. That is, the K-M test does not identify a significant change for stars younger than 5 Gyr. The overall probability for stars < 5 Gyr old is 24% with 95% confidence limits of 18% and 34%, while the corresponding values for stars > 5 Gyr in age are 5.3% with 95% confidence limits of 1.8% and 14%. The drop in incidence of excesses is a factor of 4.5, at greater than 2σ significance. Our discussion in Section 3.3 demonstrates that errors in age or in identification of excesses are unlikely to change significantly the result that there are only four excesses in the portion of our sample older than 5 Gyr.

4.3. A Test and Confirmation

In principle, the Kaplan-Meier estimator works under the assumption of "random" censoring, i.e., that the probability of a measurement being censored does not depend on the source property being probed, in this case stellar age. We deal with debris disk measurements in terms of their significance level (e.g., χ_{70}) to allow for differing depths relative to the photosphere; about half of the sample is measured deeply enough ($\geq 3\sigma$, or $\geq 3\sigma$ on the expected photospheric level) to be detected. Thus the random censoring assumption may not be completely satisfied. For comparison, we therefore will test for the evolution of $70 \mu\text{m}$ excesses using a different method based on the shape of the probability distribution of excesses, which is also able to account for non-uniform detection limits (a similar approach has been used by Gáspár et al. (2013)). This method will also confirm that the underlying assumption for the K-M test - that the censoring is independent of age - is satisfied for our sample.

We begin by assuming that a sample of stars will have some probability distribution of excess ratios. Integrating this distribution upward from the detection threshold gives the probability that a star has a detectable excess. Lower limits for the integrals are given by:

$$LL = 1 + 3(\sigma_{70}/P_{70}) \tag{6}$$

where 1 represents the expected flux ratio of detected to photospheric flux density for no excess, σ is the uncertainty on detected flux density, F_{70} , and P_{70} is the predicted photospheric flux density. The factor of three represents the 3σ threshold placed on χ to have a significant

excess. For each star in a sample, the integral of the probability distribution from this lower limit to infinity gives the probability of detecting an excess. The values for all the stars can be summed to obtain the total number of predicted excesses in the sample. The probability distribution can be refined by adopting a number of detection thresholds and comparing the sums over the sample stars with the number of detected excesses, testing the probability distribution as a function of amount of excess. Once the final model is obtained, it can be treated as a parent distribution for comparisons with other samples of stars. That is, under the null hypothesis that a sample is identical in excess behavior to the one for which the probability distribution was determined, we can use the distribution to compute how many detections should be achieved in the second sample and compare this prediction with the number of actual detections.

To apply this approach, we evaluated several possibilities (Gaussian, lognormal, power law, and exponential) for the shape of the distribution of excess ratios for the sample of stars younger than 5 Gyr and with signal-to-noise ratios at 70 μm of at least 2 (we fitted below the $\chi = 3$ reliable detection limit to be sure the distribution was well-behaved). We refined initial guesses for the fits by computing the lower integration limit for each star, regardless of whether it was detected, as in Equation (6). We defined the upper limit for the integral to be a large enough that the value had converged. We required the sum to be 38, the total number of stars with indicated excesses ($\chi > 3$). We varied the width-parameter and the normalization constant, leaving the sum unchanged (for the Gaussian and lognormal models, we only varied the width-parameter σ and calculated the appropriate normalization factor; for the exponential and power law distributions, the exponential factor was similarly varied - it is the only other free parameter for these models). We then used least-squares minimization to fit the integral sums for each function at selected excess thresholds to the number of actual detections above that threshold. We chose 10, 20, 30, 50, 60, 90, 100, and 200, as the test thresholds. The results of these tests are given in Table 4. The lognormal and power law shapes produced the best fits. We found that the lognormal function was very consistent with the distribution of lower limits in the sample, while the power law was not. We therefore conclude that the excess ratios and lower limits are best fit with a lognormal shape:

$$\frac{C}{x\sqrt{2\pi}\sigma} e^{-\frac{(\log x - \mu)^2}{2\sigma^2}} \quad (7)$$

This result is consistent with previous work (Andrews & Williams 2005; Wyatt et al. 2007a; Kains et al. 2011; Gáspár et al. 2013) that also found that the distributions of young disk masses or excesses could be fitted with lognormal functions. To test our model, we divided the sample into two age sub-bins of 80 and 79 stars: age $<$ and \geq 750 Myr. Within these

sub-bins, 21 and 18 stars with excesses were detected, respectively. The model predicts 18.2 and 19.8 excesses for those bins, confirming the fit.

Using lower integration limits computed from the data for the stars older than 5 Gyr, the lognormal model predicts 21.6 excesses at $70 \mu\text{m}$, assuming no decay relative to the young stars. Thus, there is no significant dependence on the predicted number of excesses with stellar age; the three age divisions respectively have 18.2, 19.8, and 21.6 predicted detections, from virtually identical numbers of stars in each bin. This confirms the underlying assumption in the K-M test that the probability of censoring is not a function of stellar age.

We can also use this approach to confirm the result from the K-M test. Since only four excesses were detected, we can take the ratio of the predicted number to the detected number to obtain an estimated decay by a factor of ~ 5 . The statistical significance of this result is dominated by the poor statistics for the old star sample; it indicates a decay by a factor greater than two (2σ limit). Our modeling therefore establishes independently that debris disk excesses decay at $70 \mu\text{m}$ over time scales of 5 Gyr. Furthermore, our division of the young sample into two parts (younger and older than 750 Myr) and the finding of an equal incidence of excess in them indicates that the decay occurs late in the evolution of the debris disks, past 1 Gyr.

To place constraints on the accuracy of the model, we used a Monte Carlo approach. We created random samples of the same size as our young (< 5 Gyr) sample, using the same parameters as those in the original probability distribution. For each random sample, we recomputed the best-fit parameters. We also fit the lower limits described above to a lognormal distribution and used that distribution to generate random samples of lower limits. The recomputed fits for the random star samples and random lower limits were used to compute a predicted number of excesses for the generated random sample of stars. Over 10000 trials, the average number of excesses predicted for the young sample was 38.0 with a variance of 5.0. We repeated the procedure for the old sample by fitting the old sample lower limits to their own lognormal distribution, generating random old sample lower limits, and recomputing the fit parameters. We still used the recomputed best-fit parameters for the young star sample, and again calculated the predicted number of excesses in the old sample. The average number of excesses predicted for the random old samples was 21.6 with a variance of 1.3, over 10000 trials. The error in the predicted number of excesses is therefore dominated by the statistical uncertainty in the number of detected young stars. Combining the uncertainties quadratically, the predicted number of excesses is 21.6 ± 2.5 , confirming our 2-sigma limit is valid.

This result is in excellent agreement with the conclusions from the K-M estimator. The consistency of the two different methods gives confidence that the conclusions drawn from

the K-M estimator are correct.

5. More detailed evolution of debris disks

Another issue with previous studies (e.g., Bryden et al. (2006); Carpenter et al. (2009)) is small samples and as a result poor statistical significance; this also limits our conclusions from the *Spitzer* sample. To examine the evolution of debris disks with better statistical weight, we combine the sample described in this paper with that from DUNES (Eiroa et al. 2013) and DEBRIS (Mathews et al. 2010). We take the ages of these stars from Gáspár et al. (2013), discarding all of quality "1"; these ages were estimated as in this paper except for omission of the step to reject cases where the HR diagram and CAI were not in agreement (we therefore added a check on the HR diagram as with the *Spitzer* sample for stars older than 5 Gyr). We also take the *Spitzer*/MIPS 70 μm and DEBRIS 100 μm photometry from Gáspár et al. (2013), with the DUNES photometry from Eiroa et al. (2013). We do not consider disks possibly detected only at 160 μm (see Gáspár & Rieke (2014)), and also discard photometry listed by Eiroa et al. (2013) as likely to be confused with IR cirrus or background galaxies. We merged the measurements into a single indicator of an excess at 70 - 100 μm , and determined the significance of each excess as a χ value analogous to the definition in equation (5) (see Gáspár et al. (2013)).

5.1. Behavior of DEBRIS and DUNES Samples

The number of stars in the combined DEBRIS and DUNES samples within the relevant range of spectral types and with valid ages is 231, nearly as large as the purely *Spitzer* one. We have therefore first analyzed it independently as a check of the results in the preceding section. In this case, to divide the sample into thirds, we adopt age ranges of 0 - 1500 Myr, 1500 - 5000 Myr, and > 5000 Myr. For excesses with $R > 1.5$, we find the detection probabilities are respectively 17% (95% confidence limits of 10% and 28%), 19% (limits of 11% and 19%) and 11% (limits of 5% and 21%). These values are in agreement with those from the *Spitzer* sample, although a bit lower and hence the drop in the incidence of excesses in the oldest age range is also indicated but at a slightly less statistically significant level (slightly less than 2σ). The overall similarity of the two samples is not surprising, given that they include virtually identical numbers of stars and that the numbers of infrared excesses detectable by *Spitzer*/MIPS and *Herschel*/PACS are also similar (see Gáspár et al. (2013)).

Again, this conclusion rests on the reliability of the assigned ages, so we review those

for the old stars (i.e., indicated ages > 2500 Myr) with excesses. The following twelve stars have at least four independent age determinations (e.g., four measurements of the CAI) and should have relatively reliable ages: from DUNES, *HIP 14954*, F8V, 4500 Myr; *HIP 15372*, F2V, 4000 Myr; *HIP 32480*, G0V, 5000 Myr; *HIP 65721*, G4V, 8300 Myr; *HIP 73100*, F7V, 4000 Myr; *HIP 85235*, K0V, 5600 Myr; *HIP107649*, G2V, 4000 Myr; and from DEBRIS, *HD 7570*, F9V, 5300 Myr; *HD 20010*, F6V, 4800 Myr (there is only one measurement of the CAI, but multiple measurements put $\log g < 4$); *HD 20794*, G8V, 6200 Myr; *HD 102870*, F9V, 4400 Myr; and *HD 115617*, G7V, 5000 Myr. The number of determinations for the following three stars are lower, but there is no credible evidence that the age estimates are seriously incorrect: *HIP 27887* K2.5V, DUNES, 5500 Myr; *HIP 71181* K3V, DUNES, 3000 Myr; and *HD 38393* F6V, DEBRIS, 3000 Myr. Based on their positions on the HR diagram and a review of other data, we revised the age in Gáspár et al. (2013) for *HIP 32480*, G0V, from 5000 to 3000 Myr and for *HIP 62207*, G0V, from 6400 to 1000 Myr. The CAI age of *HD 61421*, F5 IV-V, from DEBRIS, 2700 Myr, is rather uncertain because it has a highly variable activity level (Isaacson & Fischer 2010), but its position on the HR diagram is roughly in agreement with the assigned age. In summary, the great majority of the relatively old stars with excesses appear to have reliable age estimates. as was also the case for the *Spitzer* sample. These stars are also distributed over the full range of spectral types in the sample.

5.2. Combined Sample

Because of the similarity in behavior between the *Spitzer* and *Herschel* samples, we can combine them directly. We now use this combined sample to obtain a more detailed picture of the evolution of the far infrared emission by debris disks. First, we will test for the overall evolution between the incidence of excesses in young and old disks. Below, we will justify a division between a "young" sample with ages < 3000 Myr and an "old" one with ages > 4500 Myr, with the gap left as a transition. There are 235 stars in the first and 168 in the second category. We compute the excess probabilities based on different threshold values of R , and Table 5 shows the results. With the added statistical weight from combining the two samples, there is a well-detected drop in the incidence of excesses with age. The result is seen at all of the excess-detection thresholds (i.e., all values of R), although it becomes stronger for larger excesses. At the lowest threshold, $R = 1.5$, it is significant roughly at a level of 5.5σ .

Two thirds of this combined sample are detected at $\geq 3 \sigma$ (or have photospheric levels that correspond to 3σ or greater), reducing the probability of censoring biases. Nonetheless,

we repeated the confirmation test described in Section 4.3 for the merged sample⁴. The model shows that the combined sample is uniform in overall sensitivity to debris disk excesses across the entire age range (e.g., fitted values of 34 - 35 excesses in each of the younger and older halves of the "young sample" and to the "old" sample). The prediction of 35 for the old sample with a variance by the Monte Carlo simulation of 2.2 is significantly larger than the observed number of 11. The probability of this outcome (computed from the binomial distribution) if there is no evolution is $< 2 \times 10^{-7}$, or equivalently it is a $> 5 \sigma$ indication of evolution.

Given the confirmation of the K-M results and the strong indication of evolution, we applied the K-M approach to estimate the incidence of debris excesses as a function of age. We have used an 80-star running average of the combined sample to determine the most probable incidence of excesses for various values of R. The results are displayed in Figure 7 and selected values are listed in Table 6. As shown by the 1- σ error zones, the individual bumps and wiggles in the curves are not significant. The important characteristics of the behavior are: 1.) the very large excesses decline more rapidly than smaller ones; 2.) small excesses ($R \sim 2$) persist at a more-or-less constant incidence up to an age of ~ 3000 Myr; 3.) there is a decline in the incidence of excesses between 3000 and 5000 Myr; and 4.) there is a persistent (but spectral-type-independent) incidence of excesses for stars older than 5000 Myr, even though an extrapolation of the decay from 3000 to 5000 Myr would suggest they should be rare.

Previous work has found hints of the overall reduction of excesses at old ages, but has been hampered by inadequate statistics (e.g., Bryden et al. (2006); Carpenter et al. (2009), or by a number of excesses attributed to very old stars that contradicted the trend (Trilling et al. 2008). The larger sample, higher quality measurements, and emphasis on accurate age determination can account for the trend seen clearly in our study whereas there were only hints in these previous ones.

In comparing these results with theoretical predictions, we take a fiducial debris disk radius of 30 AU (Gáspár et al. 2013) and a typical cold disk temperature of 60K (Ballering et al. 2013). From the latter, we can estimate fractional excesses corresponding to values of R as listed in Table 7. At $R = 2$, the constant level of excess up to a drop between 3000 and 5000 Myr is then in approximate agreement in pattern of behavior with the simple models for steady-state disk evolution in Wyatt (2008), Figure 5. A quantitative comparison with our results, however, cannot be made with the predicted decay for a single disk; a

⁴The different distribution of ages in the combined sample, together with the more rapid evolution for large excesses, results in a different log-normal fit.

synthesis over a population of disks is required. Figure 7 shows such a model. It is for a population of debris systems around G0V stars with an initial mass distribution width as in Andrews & Williams (2005) with a median mass of 5.24×10^{-6} Earth masses (integrated up to particles of 1mm radius). The debris is placed at a distance of 32.5 AU from the stars in narrow rings (10% width and height) and with optical and mechanical properties for icy grains. Details of the model are as in Gáspár et al. (2013). This model matches the initial relatively constant incidence of disks up to ~ 3 Gyr and the decay from that age to ~ 5 Gyr well. However, it falls well below the observations at ages > 5 Gyr. In general, the decay timescale is roughly inversely proportional to fractional excess, but with indications of more excesses than predicted for old stars. It is likely that the oldest disks represent late phases of dynamical activity, as derived also by Gáspár et al. (2013) with a detailed digital model of steady-state evolution that reproduces the number of excesses but yields a distribution of excess amounts that falls significantly short of the observations.

6. Conclusions

We present a sample of 238 F4 - K2 stars with high-quality *Spitzer* observations through $70 \mu\text{m}$, and for which we have been able to determine accurate ages from the chromospheric activity index, X-ray emission, and placement on an HR-diagram. Consistent with previous work, we find that the incidence of excesses at $24 \mu\text{m}$ decays dramatically from $13.6 \pm 2.8 \%$ for stars < 5 Gyr in age to none for older stars. At $70 \mu\text{m}$, we also find a significant reduction in the incidence of excesses, from 38, or $22.5 \pm 3.6 \%$ to 4, or $4.7^{+3.7}_{-2.2} \%$. We have evaluated the significance of this apparent reduction in the incidence of $70 \mu\text{m}$ excesses in two ways, both of which correctly account for the variable detection limits and resulting censoring of the data. The first is the traditional Kaplan-Meier test, which indicates a decay by greater than 2σ significance, nominally by a factor of 4.5. In the second method, we determined the distribution of excess ratios among the young (ages < 5 Gyr) stars and assumed it could be treated as a probability distribution to determine if a specific star is likely to have an excess above its individual detection limit. This model was used to predict the number of excesses that would have been detected in the old (> 5 Gyr) sample if they behaved identically to the young sample. This approach also predicts a decay at greater than 2σ significance, and nominally by a factor of five. The two methods therefore agree well on the existence and amount of this decay. Within this sample, there are two stars with excesses at $24 \mu\text{m}$ but no strong excess at $70 \mu\text{m}$, HD 1466 and HD 13246.

We then combined the *Spitzer*-only stars with the measurements for the DEBRIS and DUNES programs (for the former using both *Spitzer* and *Herschel* data to improve the

weight of the measurements). This combined sample is doubled in size, allowing us to reach robust conclusions about debris disk evolution in the far infrared. Within this larger sample, we examine the relative incidence of excesses around stars of types F4 - K4, finding no statistically significant trend with spectral type. We therefore analyze the evolution of the entire sample together. We find that, at fractional debris disk luminosity of just under 10^{-5} , the incidence of far infrared excesses declines significantly between 3000 and 5000 Myr, while for fractional luminosity of just under 10^{-4} , the decline is at an order of magnitude younger ages. This behavior is consistent with a theoretical model for passive disk evolution. However, there appear to be more excesses for the oldest stars than predicted by passive-evolution models. These excesses are distributed over the full range of spectral types in our sample. This behavior suggests that the oldest debris disks are activated by late-phase dynamical activity.

We thank the anonymous referee for a very helpful report, and the editor for suggesting improved statistical approaches. We have made use of the SIMBAD database and the VizieR catalog access tool, operated at CDS, Strasbourg, France. We have also used data products from the Two Micron All Sky Survey, which is a joint project of the University of Massachusetts and the Infrared Processing and Analysis Center/California Institute of Technology, funded by the National Aeronautics and Space Administration and the National Science Foundation. This work is also based, in part, on observations made with *Spitzer Space Telescope*, which is operated by the Jet Propulsion Laboratory, California Institute of Technology under NASA contract 1407. We thank Patricia Whitelock and the South African Astronomical Observatory for assistance and use of facilities to obtain near infrared photometry. This work supported by contract 1255094 from Caltech/JPL to the University of Arizona. JMS is supported by the National Science Foundation Graduate Research Fellowship Program, under grant No. 1122374.

REFERENCES

- Allen, D. S., & Gallagher, J. S. 1983, MNRAS, 203, 777
- Alonso, A., Arribas, S., & Martinez-Roger, C. 1998, A&AS, 131, 209
- Ammons, S. M., Robinson, S. E., Strader, J., Laughlin, G., Fischer, D., & Wolf, A. 2006, ApJ, 638, 1004
- An, D., Terndrup, D., & Pinsonneault, M. 2007, ApJ, 671, 1640
- Andrews, S. M. & Williams, J. P. 2005 ApJ, 631, 1134

- Aumann, H. H., & Probst, R. G. 1991, *ApJ*, 368, 264
- Ballering, N. P., Rieke, G. H., Su, K. Y. L., & Montiel, E. 2013, *ApJ*, in press
- Beichman, C. A., et al. 2006, *ApJ*, 652, 1674
- Bonatto, Ch., Bica, E., & Girardi, L. 2004, *A&A*, 415, 571
- Bouchet, P., Schmider, F. X., & Manfroid, J. 1991, *A&AS*, 91, 409
- Bryden, G. et al. 1999, *ApJ*, 514, 344
- Bryden, G. et al. 2006, *ApJ*, 646, 1038
- Bryden, G. et al. 2009, *ApJ*, 705, 1226
- Buccino, A. P., & Mauas, P. J. D. 2008, *A&A*, 483, 903
- Carpenter, J. M. 2001, *AJ*, 121, 2851
- Carpenter, J. M. et al. 2009, *ApJ*, 514, 344
- Carter, B. S. 1990, *MNRAS*, 242, 1
- Chen, C. H., Jura, M., Gordon, K. D., & Blaylock, M. 2005, *ApJ*, 623, 493
- Chen, C. H. et al. 2006, *ApJS*, 166, 351
- Clarke, C. J. et al. 2001, *MNRAS*, 328, 485
- Donaldson, J. K. 2012, *ApJ*, 753, 147
- Eiroa, C., et al. 2013, *A&A*, 555, 11
- Engelbracht, C. W. et al. 2007, *PASP*, 119,994
- Feigelson, E. D., & Babu, G. J. 2012, "Modern Statistical Methods in Astronomy," Cambridge; Cambridge University Press
- Fischer, D. A., & Valenti, J. 2005, *ApJ*, 622, 1102
- Gašpař, A., Rieke, G. H., & Balog, Z. 2013, *ApJ*, 768, 25
- Gaspar, A., & Rieke, G. H. 2014, *ApJ*, in press
- Glass, I. S. 1974, *MNSSA*, 33, 53

- Gordon, K. D. et al. 2005, PASP, 117, 503
- Gordon, K. D. et al. 2007, PASP, 119, 1019
- Gray, R. O., Corbally, C. J., Garrison, R. F., McFadden, M. T., & Robinson, P. E. 2003, AJ, 126, 2048
- Gray, R. O. et al. 2006, AJ, 132, 161
- Habing, H. et al. 1999, Nature, 401, 465
- Habing, H. et al. 2001, A&A, 365, 545
- Harmanec, P. 1998, A&A, 335, 173
- Henry, T. J., Soderblom, D. R., Donahue, R. A., & Baliunas, S. LO. 1996, AJ, 111, 439
- Holmberg, J., Nordström, B., & Andersen, J. 2009, A&A, 501, 941
- Isaacson, H. & Fischer, D. 2010, ApJ, 725, 875
- Jenkins, J. S. et al. 2006, MNRAS, 372, 163
- Johnson, H. L., Mitchell, R. I, Iriarte, B., & Wisniewski, W. Z. 1966a, Comm. Lun. & Plan. Lab., 4, 99
- Johnson, H. L. 1966b, ARAA, 4, 193
- Johnson, J. A., Aller, K. M., Howard, A. S., & Crepp, J. R. 2010, PASP, 122, 905
- Kains, N., Wyatt, M. C., & Greaves, J. S. 2011, MNRAS, 414, 2486
- Karatas, Y., Bilir, S., & Schuster, W. J. 2005, MNRAS, 360,1345
- Kasova, M. M., & Livshits, M. A. 2011, Ash, 88, 1217
- Kidger, M. R., & Martín-Ruiz, F. 2003, AJ, 125, 3311
- Koen, C., Marang, F., Kilkenny, D., & Jacobs, C. 2–7, MNRAS, 380, 1433
- Koerner, D. W. et al. 2010, ApJL, 710, 26
- Li, Z., Han, Z., & Zhang, F. 2007, A&A, 464, 853
- Low, F. J., Smith, P. S., Werner, M. W., Chen, C., Krause, V., Jura, M., & Hines, D. C. 2005, ApJ, 631, 1170

- Lowry, R. 2013, <http://www.vassarstats.net/index.html>
- Maldonado, J., Eiroa, C., Villaver, E., Montesinos, B., & Mora, A. 2012, *A&A*, 541, 40
- Mamajek, E. E., & Hillenbrand, L. A. 2008, *ApJ*, 687, 1264
- Mamajek, E. E. 2009, *Proc. IAU*, 258, 375
- Marigo, P. et al. 2008, *A&A*, 482, 883
- Marsakov, V. A. & Shevelev, Yu. G. 1995, *BICDS*, 47, 13
- Martinez-Arnáiz, R., Maldonado, J., Montes, D., Eiroa, C., & Montesinos, B. 2010, *A&A*, 520, 79
- Masana, E., Jordi, C., & Ribas, I. 2006, *A&A*, 450, 735
- Matthews, B. C. et al. (2010), *A&A*, 518, 135
- Meyer, M. et al. 2006, *PASP*, 118, 1690
- Mishenina, T. V., Gorbaneva, T. I., Basak N. Yu., Soubiran, C., & Kovtyukh, V. V. 2011, *ARep*, 55, 689
- Moor, A. et al. 2009, *ApJL*, 700, L25
- Moor, A. et al. 2011, *ApJS*, 193, 4
- Montes, D. et al. 2001, *MNRAS*, 328, 45
- Newcombe, R. G. 1998, *Statistics in Medicine*, 17, 857
- Ng, Y. K., & Bertelli, G. 1998, *A&A*, 329, 943
- Plavchan, P., Werner, M. W., Chen, C. H., Stapelfeldt, K. T., Su, K. Y. L., Stauffer, J. R., & Song, I. 2009, *ApJ*, 698, 1068
- Rieke, G. H. et al. 2005, *ApJ*, 620, 1010
- Rieke, G. H. et al. 2008, *AJ*, 135, 2245
- Rizzuto, A. C., Ireland, M. J., & Robertson, J. G. 2011, *MNRAS*, 416, 3108
- Rocha-Pinto, H. J., & Maciel, W. J. 1998, *MNRAS*, 298, 332
- Rodriguez, D. R., & Zuckerman, B. 2012, *ApJ*, 745, 147

- Schmitt, J. H. M. M., & Liefke, C. 2004, *A&A*, 417, 651
- Schröder, C., Reiners, A., & Schmitt, J. H. M. M. 2009, *A&A*, 493, 1099
- Selby, M. J., et al. 1988, *A&AS*, 74, 127
- Sheehan, C. K. W., Greaves, J. S., Bryden, G., Rieke, G. H., Su K. Y. L., Wyatt, M. C., & Beichman, C. A. 2010, *MNRAS*, 408L, 90
- Soubiran, C., Le Campion, J.-F., Cayrel de Strobel, G., & Caillo, A. 2010, *A&A*, 515, 111
- Tera, F., Papanastassiou, D. A., & Wasserburg, G. J. 1974, *E&PSL*, 22, 1
- Tetzlaff, N., Neuhäuser, R., & Hohle, M. M. 2011, *MNRAS*, 410, 190
- Tokunaga, A. T. 2001, in "Allen's Astrophysical Quantities," 4th Ed., edited by A. N. Cox
- Trilling, D. E., et al. 2007, *ApJ*, 658, 1289
- Trilling, D. E., et al. 2008, *ApJ*, 674, 1086
- UKIRT 1994: http://www.jach.hawaii.edu/UKIRT/astronomy/calib/phot_cal/bright_stds.html
- Urban, L. E., Rieke, G. H., Su, K. Y. L., & Trilling, D. E. 2012, *ApJ*, 750, 98
- Valenti, J. A. & Fischer, D. A. 2005, *ApJS*, 159, 141
- Van Leeuwen, F. 2007, "Hipparcos, the New Reduction of the Raw Data," *Astrophysics and Space Science Library*, Vol. 350 (Springer)
- Voges, W. et al. 1999, *A&A*, 349, 389
- Voges, W. et al. 2000, *IAU Circ.* 7432, 1
- White, R. J., Gabor, J. M., & Hillenbrand, L. A. 2007, *AJ*, 133, 2524
- Williams, J. P., & Cieza, L. A. 2011, *ARAA*, 49, 67
- Wright, J. T., Marcy, G. W., Butler, R. P., & Vogt, S. S. 2004, *ApJS*, 152, 261
- Wright, J. T., Upadhyay, S., Marcy, G. W., Fischer, D. A., Ford, E. B., & Johnson, J. A. 2009, *ApJ*, 693, 1084
- Wyatt, M. C. 2007, *ApJ*, 663, 365
- Wyatt, M. C. et al. 2007, *ApJ*, 658, 569

Wyatt, M. C. 2008, *ARAA*, 46, 339

Zuckerman, B., & Song, I. 2004, *ARAA*, 42, 685

Zuckerman, B., Rhee, J. H., Song, I., & Bessell, M. S. 2011, *ApJ*, 732, 61

Table 1. Sources of Data

PID	number of stars	sample description	source
41	66	unbiased sample of F5-K5 stars (selection on expected photospheric brightness as well as spectral type), supplemented by stars with radial velocity planets but otherwise similar	Trilling et al. (2008)
52	1	volume limited sample , with additional constraints on predicted flux and backgrounds	program abstract
54	1	A3-F8 stars in binary systems, selected for proximity, binary characteristics, low IR background	Trilling et al. (2007)
72	8	young based on lithium, H α , X-rays, or membership in TW Hya	Low et al. (2005)
80	10	A through M-type dwarfs selected on the basis of probable youth from lithium abundance, X-ray emission, chromospheric activity, and rotation	Plavchan et al. (2009)
84	3	F, G, and K stars indicated to be members of Sco/Cen based on Hipparcos	Chen et al. (2005)
148	78	unbiased sample from 3 Myr to 3 Gyr in estimated age, equally distributed over this range, masses between 0.7 and 1.5 M $_{\odot}$ (roughly F2V - K5V)	Meyer et al. (2006)
206	1	eight members of Castor Moving Group, no preselection for excesses	program abstract
713	1	member of Trilling et al. sample (PID 41) observed in IOC	Trilling et al. (2008)
2324	14	potential TPF target stars, spectral types F0 - M3.5, no companions within 100pc, terrestrial planet zone exceed 50 mas, generally within 25 pc	Beichman et al. (2006)
3401	1	F-type stars with some previous indication of IR excess preferred; this star has a 60 μ m IRAS detection	Moor et al. (2011)
3600	3	members of nearby young associations	Zuckerman et al. (2011)
20065	1	thirteen CoROT target stars	program abstract
20707	1	selected <i>either</i> for IRAS detection <i>or</i> for membership in young associations; since the star in question has no IRAS excess (and no 70 μ m excess), there is no bias	Moor et al. (2009)
30211	5	unbiased sample of F5 - F9 stars older than 1 Gyr	Trilling et al. (2008)
30339	2	fifteen thick disk stars within 40 pc (volume limited)	Sheehan et al. (2010)
30490	57	volume limited sample within 25 pc	Koerner et al. (2010)
40078	2	stars selected on the basis of tight binarity (≤ 3 AU), A3 - F8 types	program abstract

Table 2. *Spitzer* Star Sample

HD	ST ^a	Age MYr	Ref. ^b	π (mas)	[Fe/H] (dex)	V (mag)	K_S (mag)	Ref. ^c	PID	AORKey	F_{24} (error) (mJy)	F_{70} (error) (mJy)
105	G0V	170	1,2,3,4,5,6	25.4	-0.23	7.51	6.12	1	148	5295872	27.82 (0.30)	152.70 (9.71)
377	G2V	220	1,3,7,5,6	25.6	-0.10	7.59	6.12	1	148	5268992	36.31 (0.39)	170.60 (10.62)
870	K0V	2300	2,8	49.5	-0.20	7.22	5.38	1	30490	19827456	49.75 (0.51)	22.51 (4.98)
984	F5	250	1,3,6,7	21.2	-0.11	7.32	6.07	1	148	5272064	26.51 (0.29)	-7.78 (5.57)
1237	G8.5Vk:	300	1,2,6,8	57.2	-0.09	6.59	4.86	1	41	4060672	84.41 (0.85)	11.81 (2.08)
1461	G0V	7200	3,5,9	43.0	0.09	6.47	4.897	1	30490	19886336	80.19 (0.35)	61.43 (6.08)
1466	F9V	200	2,6	24.1	-0.27	7.46	6.15	1	72	4539648	34.47 (0.36)	16.83 (3.09)
2151	G0V	7000	2,8,15,17	134.1	-0.03	2.82	1.286	2,3,4,5	30490	19759616	2225.00 (1.17)	250.70 (5.26)
4307	G0V	8100	3,5,8	32.3	-0.23	6.15	4.622	1	41	4032512	103.00 (0.60)	9.58 (3.21)
4308	G6VFe-09	5700	2,6,8	45.3	-0.34	6.55	4.945	1	30490	19752192	75.79 (0.32)	6.86 (4.67)
4614	G0V	5400	3,5,11	168.0	-0.30	3.46	1.930	6,7	52	4208896	1153.00 (4.89)	125.60 (5.85)
6611	F5	5900	3	19.4	-0.13	7.24	5.913	1	30211	17345536	30.29 (0.24)	0.15 (2.40)
6963	K0V	1300	3,5,6,7,9	36.9	...	7.66	5.94	1	148	5396224	32.45 (0.34)	41.37 (5.05)
7193	F5	590	6	29.2	-0.32	6.89	5.66	1	30211	17335808	43.47 (0.47)	12.98 (4.25)
7590	G0	550	3,5,6,9,10	43.1	-0.28	6.59	5.18	1	80	4634624	62.56 (0.64)	228.60 (12.59)
7661	G9Vk:	320	1,3,7,8	38.6	-0.08	7.55	5.74	1	148	5371136	35.88 (0.38)	7.05 (5.27)
8574	F8	6700	3,5,11	22.4	-0.13	7.12	5.784	1	41	4005376	34.67 (0.19)	4.62 (2.02)
8907	F8	550	3,6,10	28.8	-0.25	6.66	5.42	1	148	5362432	51.19 (0.52)	270.30 (14.23)
9540	G8.5V	1500	1,3,5,6,8,10,11,12	52.5	-0.10	6.97	5.16	1	30490	19872256	60.42 (0.61)	-2.26 (4.90)
10086	G5IV	1300	3,5,6,9	46.8	0.02	6.60	4.98	1	30490	19852544	72.30 (0.73)	7.73 (5.32)
10647	F9V	1900	1,8,12	57.4	-0.13	5.52	4.23	2	713	7865856	196.20 (1.96)	1035.00 (52.07)
10697	G5IV	8000	3,5,11	30.7	0.06	6.27	4.601	1,8,9	41	4033792	100.50 (0.62)	0.14 (2.84)
11850	G5	1000	3,5,6,7	31.4	-0.02	7.85	6.19	1	148	5375744	23.54 (0.26)	-7.80 (4.83)
12051	G5	8000	3,5,9,	40.0	0.00	7.14	5.322	1	30490	19894016	51.79 (0.25)	0.29 (5.76)
12661	K0V	8000	3,5,11	28.6	-	7.43	5.861	1	72	4563968	32.98 (0.18)	2.69 (4.03)
13246	F8V	30	12,13	22.6	-0.17	7.50	6.20	1	20707	15009280	45.87 (0.47)	-3.06 (4.18)
13531	G0V	450	3,7,5,6,9	38.2	-0.20	7.35	5.66	1	148	5372672	39.25 (0.41)	-1.15 (4.39)
13594	F4V	600	6,14	25.3	-0.20	6.05	4.98	1	54	4236032	74.65 (0.76)	9.51 (3.12)
14082	F5V	230	3,6	29.0	-0.15	6.99	5.79	1	3600	11256064	38.54 (0.43)	1.83 (5.32)
15335	G0V	8000	3,5,15	31.8	-0.25	5.89	4.480	1	41	4035328	122.30 (0.69)	6.03 (3.51)
16141	G5IV	8500	3,5,11,16	25.7	-0.12	6.83	5.266	1	72	4562432	56.01 (0.40)	12.52 (5.32)
17051	F9Vfe+03	1200	1,2,6,8,12	58.3	0.00	5.40	4.14	1,2,10	41	4036096	170.70 (1.71)	21.94 (3.24)
18803	G8V	4500	3,5,6,9	48.5	0.12	6.62	4.95	1	30490	19886592	70.71 (0.72)	...
19019	F8	1900	3,5,6,7	32.3	-0.24	6.92	5.57	1	148	5407744	41.93 (0.44)	8.97 (5.94)

Table 2—Continued

HD	ST ^a	Age MYr	Ref. ^b	π (mas)	[Fe/H] (dex)	V (mag)	K_S (mag)	Ref. ^c	PID	AORKey	F_{24} (error) (mJy)	F_{70} (error) (mJy)
19668	G0V	200	3,5,7	26.7	...	8.48	6.70	1	148	5340928	18.54 (0.22)	-2.54 (5.46)
20367	G0	500	3,5,6,11	37.5	-0.09	6.40	5.04	1	41	12711936	68.15 (0.70)	7.01 (2.56)
20619	G0	3500	3,5,6,9,10,11	39.7	-0.27	7.05	5.47	1	30490	19847424	44.92 (0.46)	-1.52 (5.68)
20630	G5Vv	400	1,4,5,6	109.4	0.00	4.84	3.25	5,7,11	41	4036864	365.70 (3.66)	35.64 (7.14)
20766	G2V	2000	2,4,6,8,10,12	83.3	-0.31	5.53	3.96	2,3,10,11	41	4037120	195.20 (1.96)	31.27 (3.98)
20794	G8V	6700	1,2,4,8	165.5	-0.33	4.26	2.487	3,4,5	2324	10229248	758.00 (2.89)	106.70 (3.85)
20807	G0V	3000	2,4,6,8,12	83.1	-0.33	5.24	3.76	2	41	4037376	236.50 (2.37)	41.70 (3.89)
22879	F9V	6500	3,4,7,20	39.1	-0.81	6.68	5.179	1	30490	19856896	59.00 (0.28)	15.43 (5.16)
23079	F9.5V	5300	2,8,12	29.5	-0.23	7.12	5.705	1	41	4080384	36.87 (0.27)	5.06 (1.67)
23754	F5IV-V	4000	1,6,8	56.7	0.13	4.22	3.17	2	2324	10230272	392.50 (3.93)	48.81 (3.84)
25457	F5V	300	1,3,6,7,9,10,11	53.1	-0.10	5.38	4.18	1	148	5308672	207.70 (2.08)	321.70 (16.92)
26923	G0VH-04	600	6,9,8,16	46.9	-0.13	6.32	4.90	1	41	4060928	78.43 (0.81)	5.55 (2.36)
27466	G5	1500	1,3,5,7	26.2	-0.15	7.84	6.28	1	148	5412096	21.49 (0.24)	5.21 (4.73)
28185	G6.5IV-V	6600	5,8	23.6	0.12	7.80	6.185	1	41	4005632	23.97 (0.11)	0.10 (1.90)
29231	G9V	2700	1,2,7,8	35.6	0.06	7.61	5.81	1	148	5406208	33.05 (0.34)	14.73 (4.66)
30495	G1.5VH-05	700	1,2,3,5,6,8,10,11	75.3	-0.08	5.49	4.00	1	41	4037632	193.20 (1.94)	120.30 (7.07)
30649	G1V-VI	7000	3,4,5,20	33.1	-0.54	6.94	5.440	1	30339	18056960	48.23 (0.24)	0.45 (3.63)
30652	F6V	1200	1,3,6,11	123.9	-0.03	3.19	2.04	4,6,10	41	4037888	1093.00 (10.93)	129.30 (8.51)
31392	G9V	2200	2,5,7,8	39.7	0.08	7.60	5.77	1	148	5398528	36.75 (0.38)	71.12 (5.33)
33262	F9Vfe-05	500	1,6,8,10	85.9	-0.20	4.71	3.42	2	41	4038144	332.30 (3.33)	66.32 (5.89)
33636	G0VH-03	4000	3,5,8	35.3	-0.23	7.00	5.57	1	41	4059136	42.49 (0.46)	38.07 (2.42)
34411	G1.5IV-V	7700	3,5,9,11	79.2	0.05	4.69	3.248	6,7,8	41	4038656	371.30 (1.67)	0.43 (8.68)
34721	G0V	7100	3,5,8,11,15	40.0	-0.12	5.96	4.555	1	41	4038912	109.70 (0.61)	8.56 (2.67)
35114	F5/F6V	30	6,13	20.7	-0.18	7.39	6.14	1	3600	11260160	32.50 (0.35)	9.72 (4.17)
35296	F8V	300	1,6,9,16	69.5	-0.15	5.00	3.71	10	41	4061184	247.60 (2.48)	28.78 (6.17)
37006	G0	280	3,5,6,7	29.0	-0.19	8.20	6.47	1	148	5389312	18.61 (0.20)	-1.08 (4.03)
37216	G5	480	3,5,6,7	35.8	-0.02	7.85	6.00	1	148	5387008	27.67 (0.29)	7.11 (5.44)
38529	G4V	6200	1,3,5,7,11,15	25.5	0.34	5.95	4.211	1	148	5437440	150.60 (0.56)	58.70 (6.83)
38949	G1V	900	1,3,5,6,7	23.1	-0.19	7.80	6.44	1	148	5340160	19.88 (0.22)	8.59 (4.40)
40216	F6V	30	6,13	18.4	0.02	7.46	6.21	1	3600	11261952	23.92 (0.27)	-1.61 (4.24)
41700	F9VFe-04	300	2,3,5,8,11	37.6	-0.23	6.35	5.04	1	148	5365760	71.95 (0.73)	17.57 (4.15)
42807	G2V	400	4,6,9,10,16	55.7	-0.16	6.43	4.85	1	30490	19864320	78.07 (0.79)	...
43042	F6V	2300	1,6,9	48.0	0.07	5.20	4.13	1	30490	19753216	163.00 (1.65)	...
43162	G6.5V	350	3,5,6,8,11	59.8	-0.10	6.37	4.73	1	41	4039680	97.06 (0.98)	14.88 (2.55)

Table 2—Continued

HD	ST ^a	Age MYr	Ref. ^b	π (mas)	[Fe/H] (dex)	V (mag)	K_S (mag)	Ref. ^c	PID	AORKey	F_{24} (error) (mJy)	F_{70} (error) (mJy)
43989	G0	60	5,6,7	20.3	...	7.95	6.55	1	148	6598912	20.69 (0.24)	10.43 (5.18)
44770	F5V	1000	6,9	27.0	...	6.72	5.58	1	30490	19808768	41.52 (0.44)	...
45067	F9V	7100	2,3,5,8,9	29.8	-0.08	5.88	4.506	1	20065	13852416	114.00 (0.62)	15.62 (2.85)
48737	F5IV	2000	6,9,15,16,17	55.6	-0.03	3.35	2.26	6	30490	19762688	960.50 (9.61)	...
49095	F6.5V	3500	6,8	41.0	-0.18	5.92	4.66	1	30490	19766272	98.81 (0.99)	7.60 (4.75)
50692	G0V	5800	3,4,5,9	58.0	-0.25	5.74	4.293	1	41	4040192	140.10 (0.77)	9.01 (4.04)
51419	G5V	6000	9,3,5,21	40.6	-0.41	6.94	5.311	1	30490	19835136	51.95 (0.26)	9.75 (6.36)
51825	F8IV-V	300	6,14	23.2	-0.19	6.23	5.09	1	40078	21846784	64.89 (0.66)	9.97 (3.36)
55575	G0V	5700	9,3,5	59.2	-0.35	5.54	4.115	1	41	4040704	169.70 (0.85)	28.88 (3.96)
59468	G6.5V	6000	2,8,12	44.1	-0.01	6.72	5.042	1	30490	19777280	67.25 (0.29)	...
60737	G0	250	5,6,7	25.4	-0.15	7.70	6.25	1	148	5268224	23.70 (0.26)	14.80 (4.84)
61005	G8Vk+?	120	1,2,5,7,8	28.3	-0.19	8.23	6.46	1	148	5267456	45.24 (0.47)	636.20 (32.40)
62613	G8V	4100	3,4,5,6,11	58.2	-0.23	6.55	4.86	1	41	4041216	83.40 (0.85)	10.24 (2.04)
62644	G8IV-V	10100	8,15	40.5	-	5.04	3.211	10	2324	10268160	379.80 (1.64)	50.55 (4.15)
63433	G5IV	300	3,5,6,9	45.5	-0.15	6.90	5.26	1	80	4634112	58.32 (0.61)	-2.08 (5.60)
64324	G0	1300	3,5,7	29.2	-0.16	7.78	6.24	1	148	5400832	23.77 (0.27)	1.03 (5.60)
65583	G8V	6700	3,4,5,9,20	59.6	-0.71	6.97	5.095	1	30490	19837184	64.99 (0.32)	0.31 (6.54)
65907	F9.5V	3800	2,8,12	61.7	-0.34	5.59	4.24	1,3,5	30490	19750400	155.30 (1.56)	...
67228	G1IV	8900	1,3,5,9	42.9	0.07	5.30	3.801	5	2324	10267648	221.10 (1.09)	12.43 (3.54)
68017	G4V	6000	3,4,5,9,20	45.9	-0.42	6.78	5.090	1	30490	19854080	64.79 (0.31)	6.21 (6.09)
71148	G5V	5400	3,4,5,9	44.9	-0.10	6.32	4.830	1	41	4041984	83.53 (0.52)	9.65 (2.29)
72760	G5	470	3,5,6,7,9,10,11	47.3	0.01	7.32	5.42	1	80	4634368	48.48 (0.51)	5.64 (4.19)
73350	G0	750	3,5,6,9,10	41.7	0.03	6.74	5.22	1	80	4639744	64.19 (0.66)	118.30 (7.39)
75302	G0	1400	1,3,6,7	32.3	-0.07	7.45	5.84	1	148	5404672	32.82 (0.35)	-0.32 (5.22)
76151	G3V	2200	2,5,6,8	57.5	-0.04	6.01	4.46	1	41	4042752	122.30 (1.23)	32.88 (3.58)
76218	G5	550	3,5,6,7,9	38.4	-0.10	7.69	5.83	1	148	5374208	33.91 (0.36)	-8.75 (4.88)
76943	F5V	1400	6,9,17	62.2	0.07	3.96	2.88	6,10	30490	19800320	517.50 (5.18)	19.54 (26.07)
78366	F9V	800	5,6,9,10,11	52.1	-0.10	5.95	4.55	1	2324	10241280	109.20 (1.11)	17.34 (3.39)
79028	F9V	7200	1,9,17	51.1	-0.12	5.18	3.691	10	30490	19798272	245.30 (0.80)	24.39 (4.95)
81485	G3V	740	2	17.6	-0.13	8.00	6.78	1	72	4544512	14.08 (0.15)	-3.13 (3.21)
81997	F6V	1500	1,6,16	57.7	0.01	4.59	3.48	10	2324	10245632	289.80 (2.90)	33.84 (3.58)
84737	G0.5Va	9300	3,5,9	54.4	0.07	5.08	3.609	1,6	41	4043264	255.40 (1.15)	35.56 (3.94)
85301	G5	800	3,6,7	30.5	-0.03	7.74	6.09	1	148	5400064	36.41 (0.38)	33.09 (4.36)
86728	G3Va	8100	3,5,9	66.5	0.15	5.37	3.821	1	30490	19826688	210.70 (0.70)	5.50 (58.27)

Table 2—Continued

HD	ST ^a	Age MYr	Ref. ^b	π (mas)	[Fe/H] (dex)	V (mag)	K_S (mag)	Ref. ^c	PID	AORKey	F_{24} (error) (mJy)	F_{70} (error) (mJy)
88725	G1V	6000	3,4,5,16,20	28.2	-0.63	7.75	6.153	1	30339	18057728	24.31 (0.14)	2.28 (3.22)
88742	G0V	2300	1,2,6,7,8	43.8	-0.24	6.38	4.95	1	148	5422848	73.85 (0.75)	8.30 (4.99)
89269	G5	5900	3,5,9	49.4	-0.25	6.66	5.012	1	30490	19835392	69.19 (0.31)	2.51 (42.60)
89449	F6IV	3100	9,16	46.8	0.09	4.78	3.60	1	2324	10233600	241.80 (2.43)	29.10 (3.66)
90156	G5V	5900	2,3,5,8	44.7	-0.31	6.92	5.245	1	30490	19744256	55.43 (0.26)	6.39 (5.35)
90343	K0	1700	6,16	48.2	...	7.29	5.39	1	30490	19780352	50.13 (0.51)	4.63 (4.61)
90839	F8V	3100	1,3,6,9,11	78.3	-0.16	4.82	3.52	10	41	4006656	281.20 (2.82)	34.01 (4.20)
90905	F5	250	3,5,6,7	31.7	-0.10	6.88	5.52	1	148	5336320	49.24 (0.51)	18.90 (6.28)
91782	G0	400	6,7	16.3	...	8.09	6.76	1	148	5331712	14.64 (0.18)	-2.33 (4.47)
92719	G1.5V	3600	5,8	42.0	-0.21	6.79	5.26	1	30490	19885056	55.53 (0.57)	10.29 (5.84)
92788	G5	6300	1,3,5,7,11	28.2	0.16	7.31	5.721	1	148	5440512	35.96 (0.20)	3.29 (5.21)
92855	F9V	450	3,5,6,7	26.8	-0.21	7.28	5.89	1	148	5332480	31.74 (0.33)	-2.40 (3.81)
94388	F6V	3300	6,8,15	32.5	0.17	5.23	4.02	10	41	4044032	170.90 (1.72)	17.69 (3.46)
95188	G8V	270	3,5,7	27.9	...	8.49	6.65	1	148	5344768	16.16 (0.21)	-4.86 (4.64)
97334	G0V	500	5,6,9,10,16	45.6	-0.09	6.41	4.96	1	80	4640512	74.22 (0.76)	10.90 (4.66)
97343	G8.5V	6900	2,3,5,8	45.2	0.03	7.05	5.220	1	30490	19853056	56.62 (0.28)	0.26 (5.63)
98281	G8V	5300	3,5	46.4	-0.29	7.29	5.457	1	30490	19803136	45.57 (0.23)	0.29 (5.91)
99491	K0IV	4100	3,5	56.4	0.13	6.49	4.75	1	30490	19827200	91.60 (0.93)	5.90 (7.39)
101472	G0	900	3,6,7	25.5	-0.22	7.41	6.14	1	148	5343232	26.10 (0.29)	-4.76 (5.63)
101501	G8V	900	3,4,5,6,9,11	104.0	-0.12	5.31	3.59	1,6	41	4044800	261.50 (2.62)	29.01 (4.73)
101959	F9V	3800	2,3,5,7,8	30.7	-0.17	6.97	5.61	1	148	5419008	40.04 (0.41)	4.76 (4.51)
102365	G2V	6000	1,2,5,8	108.5	-0.33	4.89	3.273	3,5,11	2324	10248192	363.20 (1.49)	47.56 (4.10)
102438	G6V	5200	2,8	57.2	-0.40	6.48	4.798	1	41	4045056	86.62 (0.51)	9.96 (2.16)
103432	G0	2800	3,4,5,7	24.7	-0.18	8.20	6.55	1	148	5428992	16.76 (0.21)	1.16 (4.96)
104860	F8	250	3,5,6,7	22.0	-0.26	7.92	6.50	1	148	5270528	19.60 (0.21)	188.70 (10.22)
105631	K0V	1500	3,5,6,7,9,10	40.8	...	7.46	5.60	1	148	5415936	40.14 (0.41)	5.38 (4.10)
106252	G0V	5500	3,5,7,11	26.5	-0.15	7.41	5.929	1	148	5442816	30.24 (0.16)	4.90 (4.94)
106906	F5V	15	18	10.9	-0.01	7.80	6.68	1	84	4783872	102.10 (1.05)	285.30 (16.95)
107146	G2V	200	3,5,6,7	36.4	-0.23	7.04	5.54	1	148	5312512	62.86 (0.64)	782.20 (39.62)
108944	F8	900	7	23.6	-0.15	7.33	6.03	1	148	5334784	28.52 (0.31)	-2.37 (4.31)
109358	G0V	4900	3,5,6,7,9,11	118.5	-0.26	4.24	2.81	1	30490	19863552	557.20 (5.57)	60.03 (6.04)
111456	F5V	700	7,16,17	41.6	-0.19	5.83	4.55	1	30490	19754240	111.00 (1.11)	6.30 (4.95)
113376	G3V	5500	2	10.7	-0.24	8.48	6.702	1	84	4788736	15.09 (0.13)	0.77 (13.98)
114613	G4IV	7800	2,5,8,12,15	48.4	-	4.85	3.237	6	41	4046848	371.80 (1.71)	57.25 (4.33)

Table 2—Continued

HD	ST ^a	Age MYr	Ref. ^b	π (mas)	[Fe/H] (dex)	V (mag)	K_S (mag)	Ref. ^c	PID	AORKey	F_{24} (error) (mJy)	F_{70} (error) (mJy)
114710	G0V	4000	3,5,6,10,11,16	109.5	-0.06	4.23	2.85	6,8,12	41	4047104	516.90 (5.17)	50.47 (5.95)
114729	G0V	7200	2,3,5,8,11,20	27.7	-0.46	6.68	5.136	1	41	4084480	62.09 (0.42)	7.92 (2.23)
114853	G1.5V	5100	2,8	41.0	-0.21	6.93	5.320	1	30490	19767552	51.80 (0.26)	...
115043	G1Va	400	4,6,16	39.5	-0.22	6.82	5.33	1	148	6599168	53.62 (0.55)	8.69 (3.73)
115383	G0Vs	340	1,2,3,5,6	57.0	0.03	5.19	3.81	1	41	4047360	225.90 (2.27)	13.55 (5.11)
116956	G9V	230	9,5,6,10	46.3	-0.11	7.29	5.41	1	80	4628224	49.54 (0.51)	11.05 (5.02)
117176	G5V	8300	1,3,4,5,11,15	55.6	-0.12	4.97	3.206	1	41	4048128	385.70 (1.61)	41.18 (3.15)
119124	F7.7V	290	6,9	39.5	-0.21	6.31	5.02	1	206	6038528	73.06 (0.74)	65.47 (4.13)
121320	G0	3500	3,7,9	31.7	-0.35	7.89	6.25	1	148	5425152	22.86 (0.25)	5.91 (4.41)
121504	G2V	3500	1,2	22.2	-0.05	7.54	6.12	1	148	5438208	25.37 (0.29)	0.60 (11.01)
122652	F8	2500	3,5,6,7	25.5	-0.14	7.16	5.88	1	148	5428224	34.83 (0.36)	81.09 (6.11)
122862	F9.5V	6500	8,12	35.1	-0.21	6.02	4.580	1	41	4049152	108.60 (0.57)	12.75 (2.65)
124292	G0	6900	3,5,9	45.4	-0.15	7.05	5.304	1	30490	19880192	54.76 (0.27)	0.33 (7.03)
124425	F7Vw	2000	6,16	16.8	-0.08	5.89	4.75	1	40078	21841152	94.40 (0.96)	6.01 (3.89)
124580	G0V	940	2,8	47.1	-0.28	6.31	4.89	1	30490	19817216	80.45 (0.81)	...
124850	F7IV	2000	1,6,15,16	45.0	-0.04	4.07	2.76	1	30490	19741952	566.30 (5.67)	61.96 (7.45)
126053	G1V	5300	2,3,5,9	58.2	-0.34	6.25	4.644	1	30490	19826944	97.72 (0.41)	4.57 (6.03)
126660	F7V	500	1,6,17	68.8	-0.14	4.04	2.80	10	41	4006912	567.80 (5.68)	70.77 (6.26)
127334	G5V	8000	3,5,9	42.1	0.04	6.36	4.736	1	41	4049408	89.93 (0.51)	7.45 (2.21)
128400	G5V	800	2,6,8	50.0	-0.14	6.73	5.07	1	80	4628992	67.35 (0.69)	-1.09 (4.37)
128987	G8Vk:	500	8,5,6,10	42.2	0.02	7.24	5.53	1	80	4629248	44.36 (0.49)	-5.57 (7.44)
130948	G2V	450	2,3,5,6,10,11	55.0	-0.19	5.86	4.46	1	41	4049664	118.90 (1.20)	11.14 (2.99)
133295	F9VH-04	420	2,3,5,6,7,8	29.3	...	7.18	5.79	1	148	5367296	33.81 (0.37)	-6.14 (6.48)
134060	G0VFe+04	6500	2,8	41.3	-0.10	6.29	4.836	1	30490	19799040	80.42 (0.34)	...
134319	G5	180	3,4,5,6,7	22.4	-0.27	8.40	6.79	1	148	5307904	15.33 (0.18)	5.98 (4.01)
134987	G6IV-V	7800	3,8,5,11,12	38.2	0.20	6.47	4.882	1	41	4050432	77.79 (0.48)	4.76 (2.79)
136352	G4V	5700	1,5,12,23	67.5	-0.34	5.65	4.159	1,5,11	2324	10234880	168.20 (0.89)	18.17 (3.90)
136923	K0	3000	3,5,7,9	51.0	...	7.16	5.29	1	148	5429760	53.69 (0.55)	11.70 (4.58)
138004	G5	3800	3,5,7,9	31.1	-0.16	7.48	5.91	1	148	5433600	29.81 (0.31)	-4.26 (3.80)
140901	G7IV-V	2000	2,6,8,12	65.1	0.01	6.01	4.32	1	30490	19833088	128.70 (1.29)	...
140913	G0V	560	5,6	22.3	-0.07	8.06	6.61	1	72	4564480	16.20 (0.18)	3.79 (2.38)
141103	F5	7000	3	20.6	-0.28	6.94	5.617	1	30211	17341184	39.02 (0.30)	1.60 (3.79)
141937	G1V	4600	3,5,7,8,11	31.0	0.14	7.25	5.76	1	148	5442048	35.00 (0.37)	-1.85 (6.94)
142229	G5	330	1,3,5,6	24.5	-0.20	8.08	6.61	1	148	5385472	17.25 (0.21)	3.25 (5.53)

Table 2—Continued

HD	ST ^a	Age MYr	Ref. ^b	π (mas)	[Fe/H] (dex)	V (mag)	K_S (mag)	Ref. ^c	PID	AORKey	F_{24} (error) (mJy)	F_{70} (error) (mJy)
142860	F6IV	4600	1,3,6,11	88.9	-0.19	3.85	2.62	6,10	41	4051200	665.40 (6.66)	73.56 (7.48)
143761	G0Va	8000	3,5,9,11	58.0	-0.24	5.39	3.857	1	41	4051456	204.40 (1.00)	30.31 (4.13)
145229	G0	650	3,5,6,7	29.0	-0.28	7.45	6.00	1	148	5387776	31.18 (0.33)	66.20 (5.51)
145435	F5	6400	3	26.8	-0.19	6.69	5.325	1	30211	17336320	51.27 (0.33)	2.62 (3.90)
145675	K0V	8200	3,4,9,11	56.9	-0.05	6.61	4.714	1	41	4051712	94.20 (0.54)	10.36 (1.85)
147513	G1VH-04	1000	1,2,6,8,10	78.3	-0.13	5.37	3.93	1	2324	10244096	206.10 (2.07)	11.86 (7.42)
151541	K1V	7000	3,4	40.0	-0.28	7.56	5.687	1	30490	19793920	37.56 (0.18)	4.62 (4.71)
151798	G3V	170	1,6,7	23.8	-0.20	7.95	6.48	1	148	5276672	18.94 (0.25)	0.63 (8.24)
153458	G0	2000	1,3,6,7	22.5	0.00	7.98	6.45	1	148	5416704	18.53 (0.23)	6.45 (6.63)
153597	F6Vv	1700	6,16,17	65.5	-0.22	4.88	3.57	1	30490	19874048	273.40 (2.74)	47.22 (5.47)
154088	K0IV-V	7000	2,3,5,8	56.1	-	6.59	4.758	1	41	4061696	88.71 (0.59)	0.21 (4.35)
154417	F8.5IV-V	820	1,5,6,7,9,10,11	48.4	-0.05	6.00	4.64	1	148	5399296	101.60 (1.02)	-2.44 (6.09)
157347	G5IV	7700	3,5,9	51.2	-0.03	6.28	4.686	1	30490	19845120	91.95 (0.40)	...
157664	G0	1700	6,7	13.1	-0.23	7.96	6.70	1	148	5445888	15.43 (0.18)	0.99 (3.89)
159062	G5	6600	4,5,9,25	44.9	-0.52	7.22	5.392	1	30490	19883264	49.31 (0.23)	11.94 (5.52)
159222	G5V	4100	3,4,5,6,7,9,10,11	41.8	0.09	6.52	5.00	1	148	5436672	67.88 (0.69)	4.11 (4.59)
160691	G3IV-V	7700	2,8	64.5	-	5.12	3.570	1	41	4061952	272.10 (1.25)	31.19 (7.29)
161797	G5IV	8000	3,5,6,11	120.3	-	3.42	1.721	6,7,8	30490	19832832	1471.00 (4.55)	179.00 (5.16)
161897	K0	3000	3,5,7	33.3	...	7.60	5.91	1	148	5430528	30.33 (0.31)	-1.20 (5.55)
162003	F5IV-V	4200	6,16	43.8	-0.17	4.57	3.41	1	30490	19787520	303.20 (3.03)	47.08 (5.50)
164922	K0V	7700	3,4,5,7,9,11	45.2	0.00	7.01	5.113	1	30490	19832320	61.65 (0.27)	0.24 (4.67)
165185	G0V	500	2,6,8	57.0	-0.25	5.94	4.47	1,5,11	80	4635136	115.60 (1.17)	-5.89 (8.66)
167389	F8	1700	3,5,6,7	29.5	-0.15	7.38	5.92	1	148	5434368	29.99 (0.31)	-8.13 (4.24)
168009	G2V	7300	3,4,5,9	43.8	-0.09	6.30	4.756	1	30490	19814912	88.51 (0.35)	9.05 (5.05)
168151	F5V	2500	6,16,17	43.6	-0.22	4.99	3.83	10	41	4052480	213.70 (2.14)	24.49 (3.43)
168443	G6V	9000	3,5,8,11	26.7	-0.08	6.92	5.211	1	41	4052736	59.08 (0.40)	1.41 (26.60)
170778	G5	400	3,5,6,7	27.6	-0.18	7.49	6.05	1	148	5370368	27.26 (0.29)	-3.61 (3.58)
172649	F5	550	3,6,7	21.6	-0.24	7.50	6.23	1	148	5335552	24.18 (0.26)	-1.42 (4.44)
180161	G8V	600	3,5,60	50.0	...	7.04	5.20	1	80	4631552	59.76 (0.61)	8.62 (4.43)
181327	F5/F6V	50	13	19.3	0.07	7.04	5.91	1	72	4556032	230.30 (2.31)	1776.00 (89.31)
181655	G8V	6000	3,9,16	39.4	-0.02	6.29	4.677	1	41	4053504	94.41 (0.53)	6.18 (2.69)
182488	G8V	7100	3,4,5,9	63.5	0.03	6.37	4.493	1	2324	10243072	112.70 (0.57)	3.95 (6.55)
183216	F8.5VFe04	1000	1,2,5,6,7,8	29.1	0.05	7.13	5.77	1	148	5402368	39.13 (0.41)	23.83 (5.87)
184385	G5V	1200	3,5,9	48.6	-0.06	6.89	5.17	1	30490	19882240	60.62 (0.93)	...

Table 2—Continued

HD	ST ^a	Age MYr	Ref. ^b	π (mas)	[Fe/H] (dex)	V (mag)	K_S (mag)	Ref. ^c	PID	AORKey	F_{24} (error) (mJy)	F_{70} (error) (mJy)
186427	G3V	7600	3,5,8,9,11	47.1	-0.04	6.25	4.651	1	41	4054016	98.18 (0.55)	0.12 (2.90)
189245	F8.5Vfe-06H-05	60	1,6,8	47.1	-0.28	5.65	4.48	1	2324	10235904	124.50 (1.26)	10.59 (2.39)
190067	G7V	5300	3,5,9	52.7	-0.50	7.15	5.317	1	30490	19895552	53.62 (0.25)	...
190228	G5IV	7800	3,5,7,15	16.2	-0.36	7.30	5.352	1	148	5438976	52.23 (0.23)	34.25 (15.37)
190248	G8IV	7500	1,2,4,8,12	163.7	0.33	3.55	1.897	2,3,4,5	41	4054784	1304.00 (4.55)	142.20 (6.17)
190360	G7IV-V	8400	3,5,8,9,11,25	63.1	0.18	5.73	4.076	1	30490	19794688	167.20 (0.62)	...
190406	G0V	3500	2,3,4,5,6,8,9,11	56.3	-0.08	5.80	4.39	1	2324	10239232	129.40 (1.30)	11.22 (3.44)
190422	F9VH-04	400	2,6,8	42.7	-0.21	6.26	4.95	1	30490	19866368	77.04 (0.78)	-0.38 (6.37)
190771	G5IV	400	3,5,6,9,11	53.2	-0.02	6.18	4.62	1	30490	19767040	100.40 (1.14)	...
191089	F5V	670	6,7	19.2	-0.15	7.18	6.08	1	148	5364224	197.30 (1.98)	555.40 (28.56)
193017	F8	1450	1,3,5,6,7	25.2	0.02	7.27	5.97	1	148	5410560	29.57 (0.32)	13.51 (5.18)
195034	G5	3400	3,5,7	35.4	-0.17	7.09	5.58	1	148	5426688	42.23 (0.43)	5.11 (5.70)
195818	G0V	600	14	14.5	-0.25	8.59	7.24	1	72	4557568	9.43 (0.11)	0.59 (2.64)
196050	G3V	7400	2	20.0	0.14	7.50	6.034	1	41	12711424	27.82 (0.27)	3.18 (1.85)
199019	G5	270	3,5,6,7	28.7	...	8.23	6.48	1	148	5344000	18.91 (0.21)	-1.16 (4.86)
199260	F6V	450	5,6,8	45.5	-0.17	5.70	4.47	1,2	2324	10236672	121.80 (1.23)	45.26 (3.09)
199509	G1V	5200	3,4	42.0	-0.47	6.98	5.425	1	30490	19807744	46.59 (0.24)	5.34 (5.03)
200433	F5	1400	6	21.1	-0.11	6.91	5.85	1	30211	17343744	33.25 (0.37)	6.12 (3.29)
201219	G5	1000	3,5,6,7	26.2	0.01	8.01	6.36	1	148	5396992	22.06 (0.24)	41.46 (4.93)
202108	G0	2500	3,5,6,7,9	37.1	-0.31	7.32	5.75	1	148	5417472	35.10 (0.37)	3.64 (4.64)
202275	F5V+...	4900	9	54.1	-0.07	4.47	3.23	6	30490	19880704	366.20 (3.66)	45.14 (5.16)
202628	G1.5V	1900	2,6,8,12	41.0	-0.17	6.75	5.26	1	30490	19868160	58.83 (0.60)	106.40 (7.59)
202917	G5V	15	2,3,5,6	23.3	-0.20	8.65	6.91	1	72	4558848	20.13 (0.22)	45.52 (3.71)
203030	G8V	270	3,5,6,7	24.5	-0.03	8.45	6.65	1	148	5339392	15.59 (0.18)	3.90 (4.37)
204277	F8V	900	3,6,7	30.0	-0.16	6.72	5.45	1	148	5374976	48.84 (0.50)	27.90 (5.17)
205536	G9V	6800	2,8,12	45.4	-0.07	7.07	5.274	1	30490	19859200	53.81 (0.25)	1.33 (5.29)
205905	G1V	1250	2,3,5,6,7,8	39.0	0.05	6.75	5.32	1	148	5405440	53.01 (0.54)	17.62 (5.56)
206374	G8V	1800	3,5,6,7,9	37.1	-0.18	7.45	5.77	1	148	5415168	35.18 (0.37)	20.67 (4.38)
206860	G0VH-05	350	2,5,6,8,9	55.9	-0.16	5.96	4.56	2	41	4056832	114.00 (1.15)	25.54 (2.86)
206893	F5V	600	6,8	26.1	-0.07	6.69	5.59	1	3401	10893312	43.98 (0.46)	257.70 (15.34)
207129	G0Vfe+04	4000	2,8,12	62.5	-0.15	5.57	4.13	2,10	41	4057088	165.60 (1.66)	398.20 (21.11)
207575	F6V	30	6,13,14	22.1	-0.21	7.22	6.03	1	72	4560128	30.95 (0.32)	10.36 (2.83)
209393	G5V	500	3,5,6,7	29.6	-0.25	7.96	6.32	1	148	5368832	21.78 (0.24)	4.53 (5.00)
210277	G0V	8100	3,5,9,11	46.4	0.05	6.54	4.799	1	41	4057600	84.74 (0.52)	10.25 (2.00)

Table 2—Continued

HD	ST ^a	Age MYr	Ref. ^b	π (mas)	[Fe/H] (dex)	V (mag)	K_S (mag)	Ref. ^c	PID	AORKey	F_{24} (error) (mJy)	F_{70} (error) (mJy)
210302	F6V	4900	3,8	54.7	0.05	4.94	3.78	2,10	41	4057856	220.20 (2.21)	8.61 (5.71)
210918	G2V	7300	2,8	45.4	-0.22	6.23	4.662	1	41	4058112	99.84 (0.59)	1.70 (2.60)
212168	G0V	5600	2,8,12	43.4	-0.17	6.12	4.705	1	30490	19820288	96.26 (0.39)	0.26 (5.55)
212291	G5	3300	3,5,7	30.1	-0.28	7.91	6.27	1	148	5421312	22.66 (0.25)	2.95 (4.25)
212330	G2IV-V	7900	2,8,12	48.6	-0.14	5.31	3.71	1,2	41	4058368	246.50 (1.11)	0.23 (4.34)
213240	G0/G1V	6600	2	24.6	0.00	6.81	5.354	1	41	4080896	50.41 (0.35)	6.32 (1.67)
216437	G1Vfe+03	8000	8,12	37.4	0.07	6.04	4.518	1	41	4083968	109.90 (0.58)	9.21 (2.87)
217014	G2V+	7600	2,3,5,8,9,11	64.1	0.11	5.45	3.911	1,6	41	4058880	192.20 (0.94)	26.40 (4.75)
217343	G1.5Vk:	170	2,6,7,8	32.5	-0.22	7.47	5.94	1	148	5269760	32.22 (0.34)	5.21 (4.46)
217813	G5V	500	3,5,6,9	40.5	-0.09	6.65	5.15	1	41	4062464	61.07 (0.63)	1.62 (2.56)
218340	G3V	60	14	17.7	...	8.44	6.95	1	72	4560896	12.30 (0.14)	16.10 (2.85)
220182	K1V	350	9,3,4,5,6,9	46.5	-0.04	7.36	5.47	1	41	4062720	47.19 (0.49)	1.97 (2.66)
221420	G2IV-V	8900	8,2,12	31.8	0.19	5.82	4.32	1,2	41	4059648	139.00 (0.68)	15.89 (2.69)
222143	G4V	700	5,6,9	42.9	-0.06	6.58	5.08	1	41	4059904	68.03 (0.69)	6.03 (2.29)
222582	G5	5200	5	23.9	-	7.68	6.173	1	41	4005888	24.91 (0.15)	0.12 (2.19)
73668B	G5	2300	3,5	35.7	-0.18	8.41	6.53	1	148	9777408	17.27 (0.22)	-6.38 (6.32)
HIP6276	G9Vk:	150	3,6,7	29.1	...	8.43	6.55	1	148	5346304	19.34 (0.23)	3.33 (5.26)

^aSpectral Type

^bAge references: 1 Schroeder et al. 2009; 2 Henry et al. 1996; 3 Wright et al. 2004; 4 Rocha-Pinto & Maciel 1998; 5 Isaacson & Fischer 2010; 6 X-ray from RASS; 7 White et al. 2007; 8 Gray et al. 2006; 9 Gray et al. 2003; 10 Martinez-Arnaiz et al. 2010; 11 Kasova & Livshits 2011; 12 Jenkins et al. 2006; 13 Zuckerman & Song 2004; 14 Montes et al. 2001; 15 logg j 4; 16 Duncan et al. 1991; 17 Buccino & Mauas 2008; 18 Rizzuto et al. 2011; 19 Barrado y Navascues 1998; 20 Karatas et al. 2005; 21 Schmitt & Liefke 2004; 22 Ng & Bertelli 1998; 23 Mamajek 2009; 24 Mishenina et al. 2011

^cSources of K photometry: 1 2MASS; 2 this work; 3 Carter (1990); 4 Glass (1974); 5 Bouchet et al. (1991); 6 Johnson et al. (1966a); 7 Selby et al. (1988); 8 Kidger & Martín-Ruiz (2003); 9 Alonso et al. (1998); 10 Aumann & Probst (1991); 11 Allen & Gallagher (1983); 12 UKIRT (1994)

Table 3. Stars with Excesses

HD	Excess? ^a	$K_S - [24]$	R_{70}	χ_{70}
105	2	0.09	54.47	24.99
377	3	0.38*	80.87	26.40
870	2	-0.01	4.10	3.55
1461	2	0.02	7.10	8.65
1466	3	0.35*	5.46	5.30
6963	2	0.08	12.72	8.31
7193	1	0.11	3.04	1.76
7590	2	0.04	35.42	38.02
8907	2	0.07	52.55	49.35
10647	3	0.30*	76.26	73.02
13246	1	0.72*	0.12	-0.65
14082	1	0.11	0.61	-0.33
19668	1	0.23*	0.18	-0.26
20794	2	0.05	1.34	4.86
20807	2	0.05	1.69	4.53
25457	3	0.34	26.94	38.16
30495	2	0.08	6.08	25.69
31392	2	0.04	18.39	16.90
33262	2	0.08	1.97	5.86
33636	2	0.00	8.20	21.80
35114	1	0.28*	5.07	1.97
38529	2	0.02	3.61	6.15
43989	1	0.20*	6.55	1.63
61005	3	0.84*	483.88	102.78
73350	3	0.10	20.31	25.02
76151	2	0.04	2.53	5.99
85301	3	0.36*	15.05	7.35
90905	1	0.11	4.68	2.52
104860	2	0.09	95.37	47.48
106906	3	2.14*	230.90	30.01
107146	3	0.31*	157.49	91.11
114613	2	0.02	1.43	3.52
119124	2	0.04	8.49	22.61
122652	2	0.10	23.24	16.93
134319	1	0.12	4.38	1.10
145229	2	0.09	21.16	14.26
153597	2	-0.02	1.59	3.31

Table 3—Continued

HD	Excess? ^a	$K_S - [24]$	R_{70}	χ_{70}
181327	3	2.12*	662.75	52.66
183216	3	0.11	6.99	3.58
191089	3	2.04*	267.90	82.14
199260	2	0.05	3.54	14.36
201219	2	0.08	18.49	8.73
202628	2	0.05	19.69	15.60
202917	3	0.46*	46.44	14.92
204277	2	0.03	5.41	4.57
206374	2	0.00	5.34	3.93
206860	2	0.06	2.17	4.95
206893	2	0.06	56.49	30.30
207129	2	0.04	18.82	37.40
207575	1	0.11	3.75	2.59
218340	2	0.03	12.32	5.38
HIP6276	1	0.13	1.88	0.24

^a1 = excess at 24 μm only (or no 70 μm measurements), 2 = excess at 70 μm only, 3 = excesses at both 24 μm and 70 μm

*24 μm excess confirmed by WISE W3-W4 color.

Table 4. Probability Distribution Parameters for the *Spitzer* Sample

Shape of Fit	χ^2	Normalization	μ^{a}	σ
Power Law	20.6	0.219	1.50	-
Lognormal	6.2	0.448	1.50	2.12
Exponential	139.8	0.284	25.9	-
Gaussian	401.1	0.297	25.4	24

^a μ for the power law and exponential distributions represents the exponential factor.

Table 5. Probable Incidence of Young and Old Disks for the Combined Sample

R threshold	0 - 3000 Myr ^a	≥ 4500 Myr ^a
1.5	0.32 ^{+0.06} _{-0.06}	0.08 ^{+0.06} _{-0.03}
2	0.25 ^{+0.06} _{-0.05}	0.05 ^{+0.05} _{-0.03}
3	0.21 ^{+0.06} _{-0.05}	0.04 ^{+0.05} _{-0.02}
4	0.18 ^{+0.06} _{-0.05}	0.02 ^{+0.04} _{-0.01}
5	0.17 ^{+0.055} _{-0.045}	0.01 ^{+0.04} _{-0.01}
10	0.11 ^{+0.05} _{-0.04}	0.00 ^{+0.01} _{-0.00}

^aErrors are for 95% confidence limits.

Table 6. Probable Incidence of Disks vs. Age and R threshold^a, for the Combined Sample

Age range (Gyr)	Most probable fraction	95% confidence upper limit	95% confidence lower limit
280	0.39 .. 0.30 .. 0.19 .. 0.13	0.51 .. 0.41 .. 0.29 .. 0.22	0.29 .. 0.20 .. 0.11 .. 0.07
500	0.30 .. 0.24 .. 0.15 .. 0.11	0.41 .. 0.35 .. 0.25 .. 0.21	0.20 .. 0.16 .. 0.09 .. 0.06
850	0.21 .. 0.21 .. 0.19 .. 0.12	0.32 .. 0.32 .. 0.30 .. 0.22	0.13 .. 0.13 .. 0.12 .. 0.07
1400	0.24 .. 0.21 .. 0.15 .. 0.06	0.35 .. 0.32 .. 0.25 .. 0.15	0.15 .. 0.12 .. 0.08 .. 0.02
2200	0.32 .. 0.21 .. 0.12 .. 0.08	0.44 .. 0.32 .. 0.21 .. 0.16	0.22 .. 0.13 .. 0.06 .. 0.03
3300	0.27 .. 0.16 .. 0.08 .. 0.06	0.38 .. 0.26 .. 0.16 .. 0.15	0.18 .. 0.09 .. 0.04 .. 0.02
4450	0.12 .. 0.08 .. 0.04 .. 0.03	0.22 .. 0.17 .. 0.11 .. 0.10	0.06 .. 0.035 .. 0.01 .. 0.00
5400	0.08 .. 0.04 .. 0.01 .. 0.00	0.17 .. 0.12 .. 0.08 .. 0.06	0.03 .. 0.01 .. 0.00 .. 0.00
6300	0.09 .. 0.07 .. 0.03 .. 0.00	0.19 .. 0.16 .. 0.10 .. 0.06	0.04 .. 0.03 .. 0.01 .. 0.00
7500	0.08 .. 0.04 .. 0.01 .. 0.00	0.17 .. 0.12 .. 0.07 .. 0.06	0.04 .. 0.01 .. 0.00 .. 0.00

^aThe successive entries in each cell are for R ≥ 1.5, 2, 5, & 10.

Table 7. Approximate Fractional Excesses vs. R

R at $85\mu\text{m}$	Fractional Excess
1.5	4×10^{-6}
2	9×10^{-6}
3	1.7×10^{-5}
4	2.5×10^{-5}
5	3.5×10^{-5}
10	8×10^{-5}
15	1.2×10^{-4}
20	1.6×10^{-4}
25	2×10^{-4}

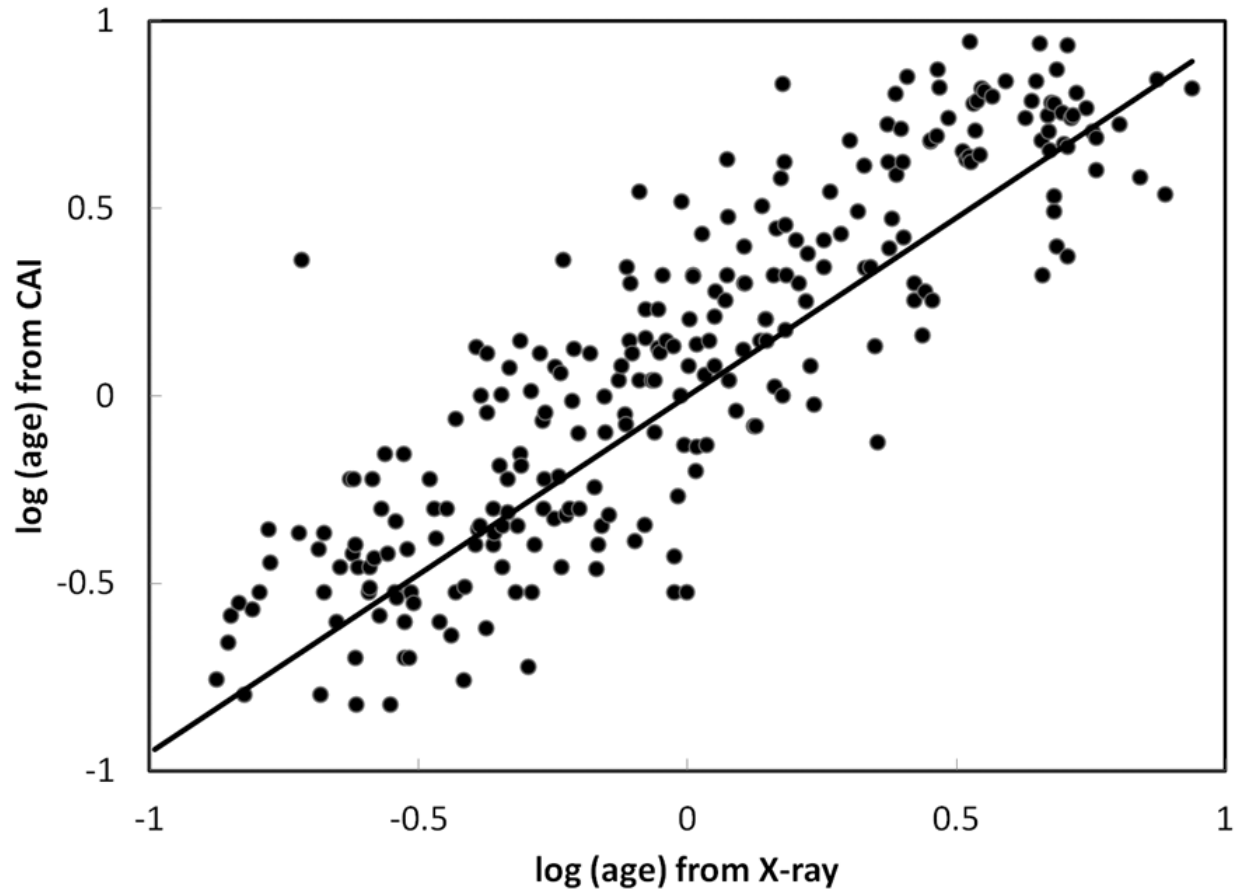


Fig. 1.— Comparison of ages (in Gyr) from the CAI with those from X-ray luminosity. The fitted line has a slope of 1.28.

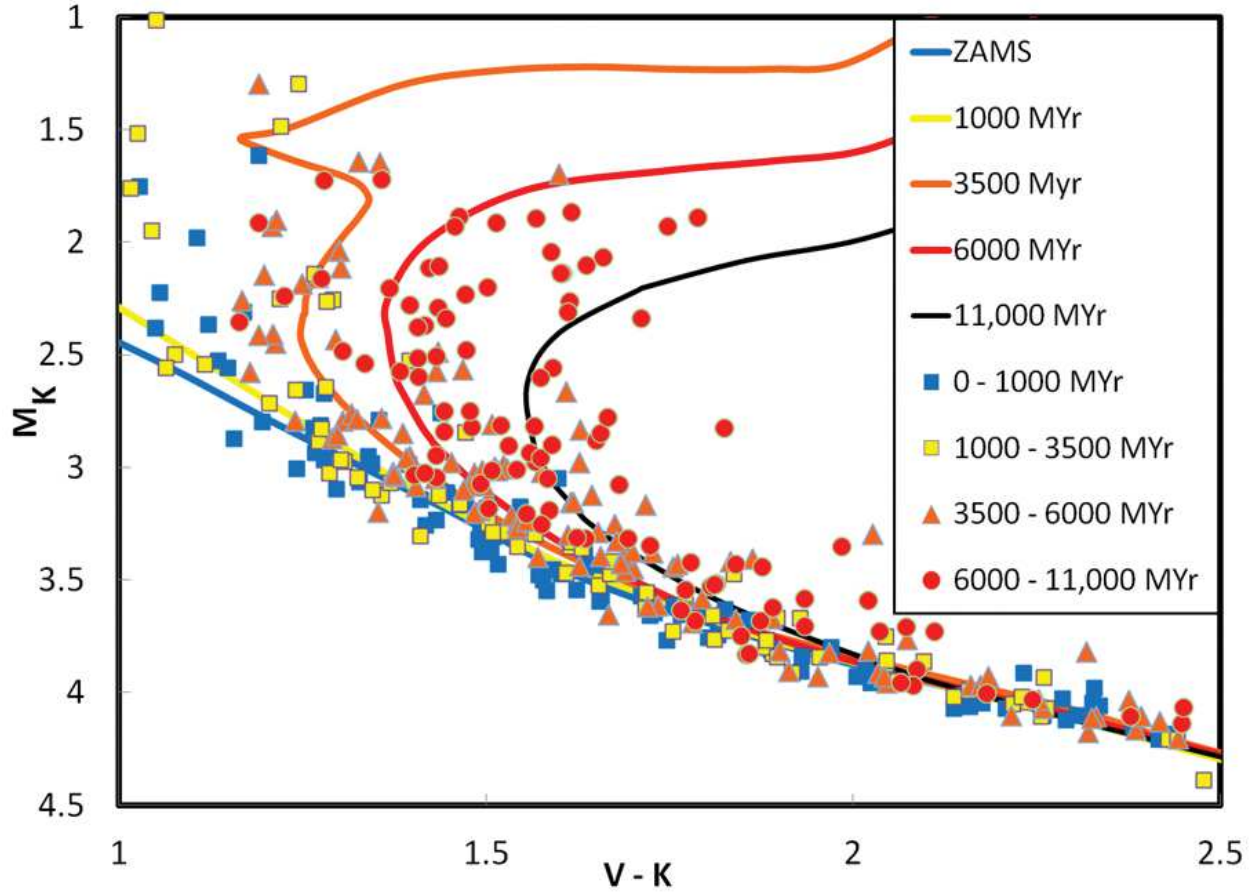


Fig. 2.— Hertzsprung-Russell diagram prepared as described in the text to compensate for stellar metallicity and to match the observational photometric system. Ages determined from the CAI are coded by the symbols and can be compared with the isochrones for various ages (Bonatto et al. 2004; Marigo et al. 2008).

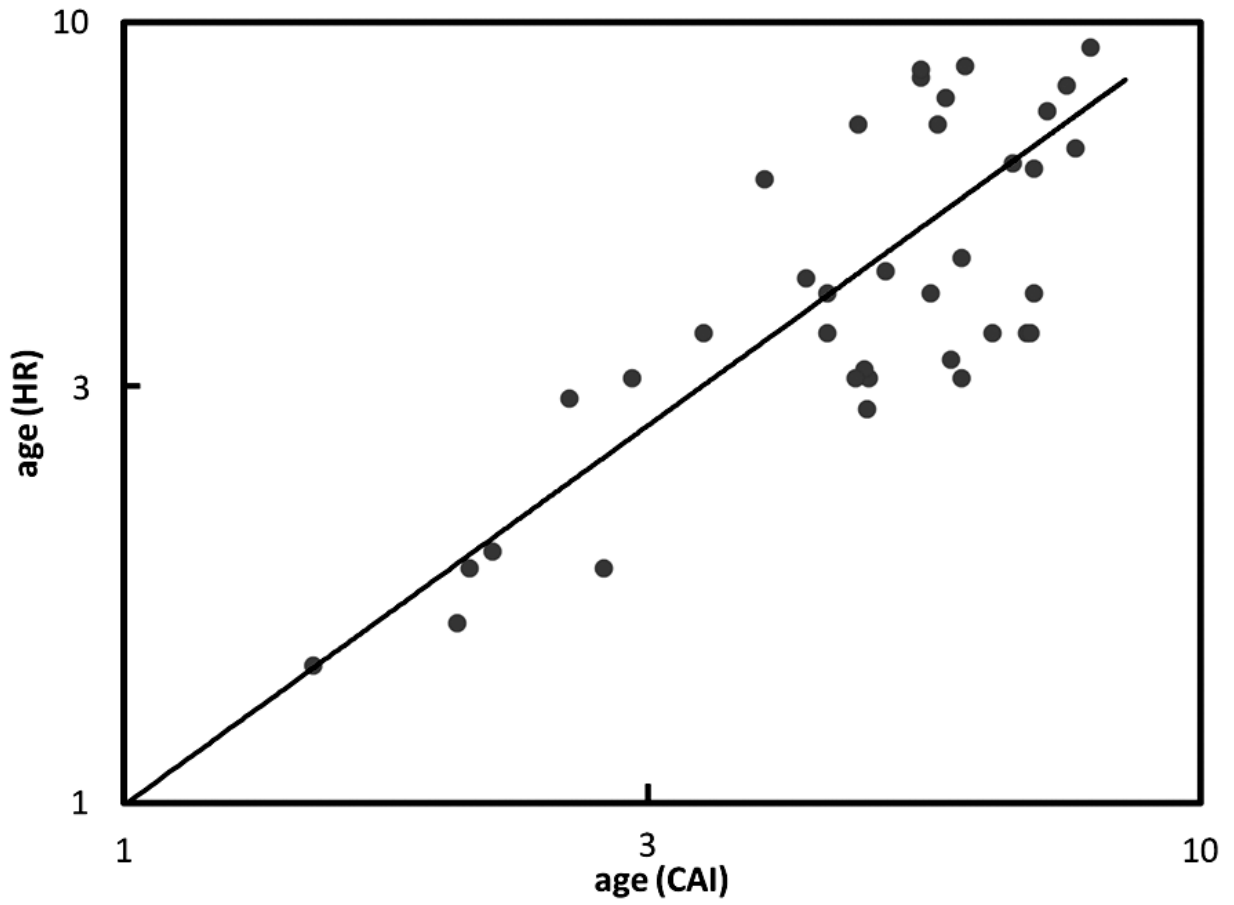


Fig. 3.— Comparison of ages (in Gyr) from the CAI and the HR diagram. The fitted line has a slope of 0.985.

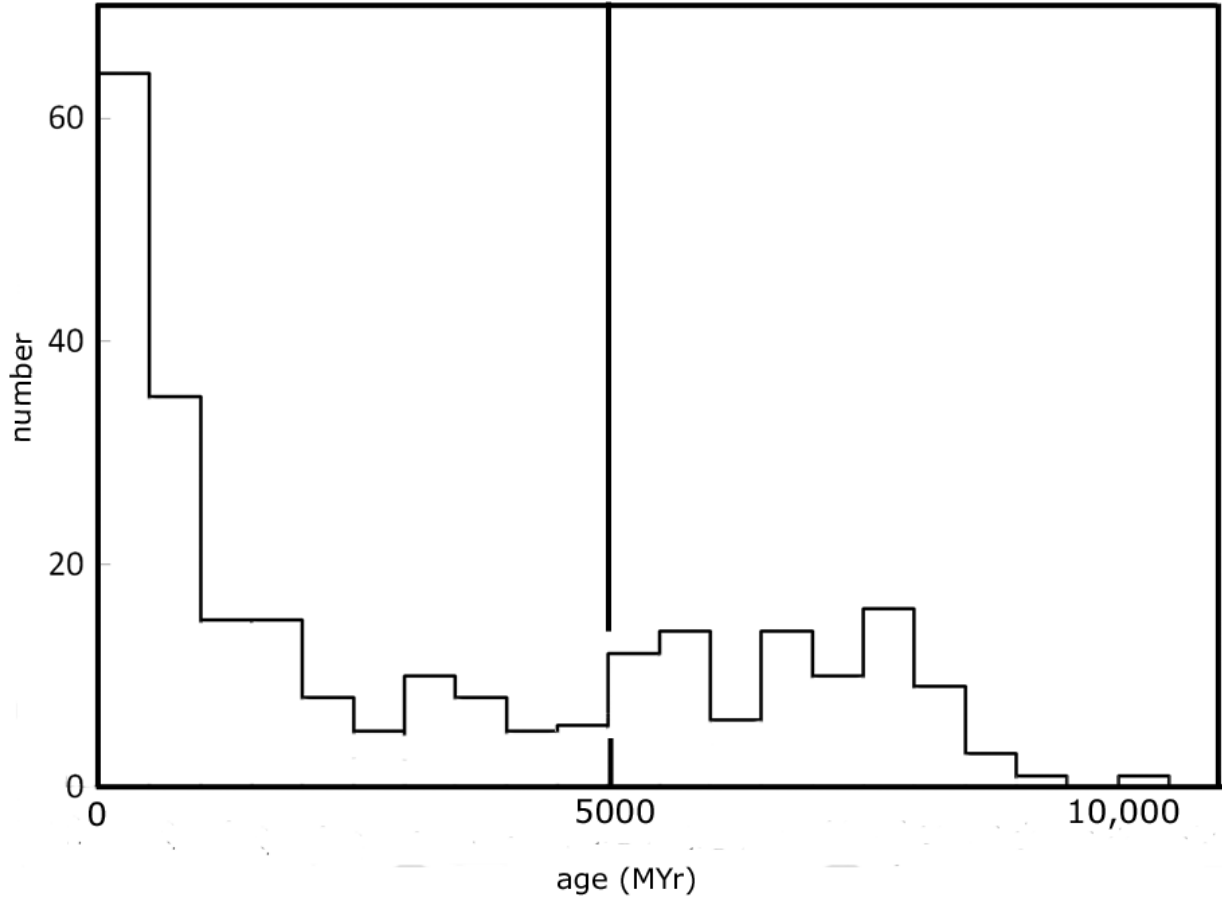


Fig. 4.— Histogram of ages in the final samples, with a bin size of 500 Myr. The vertical line indicates the minimum age for which we could apply the HR diagram criterion to confirm the stellar age. All stars to the right of this line both have ages > 5 Gyr indicated by CAI, X-ray output, $\log g$ or gyrochronology, and also fall in the appropriate region of the HR diagram.

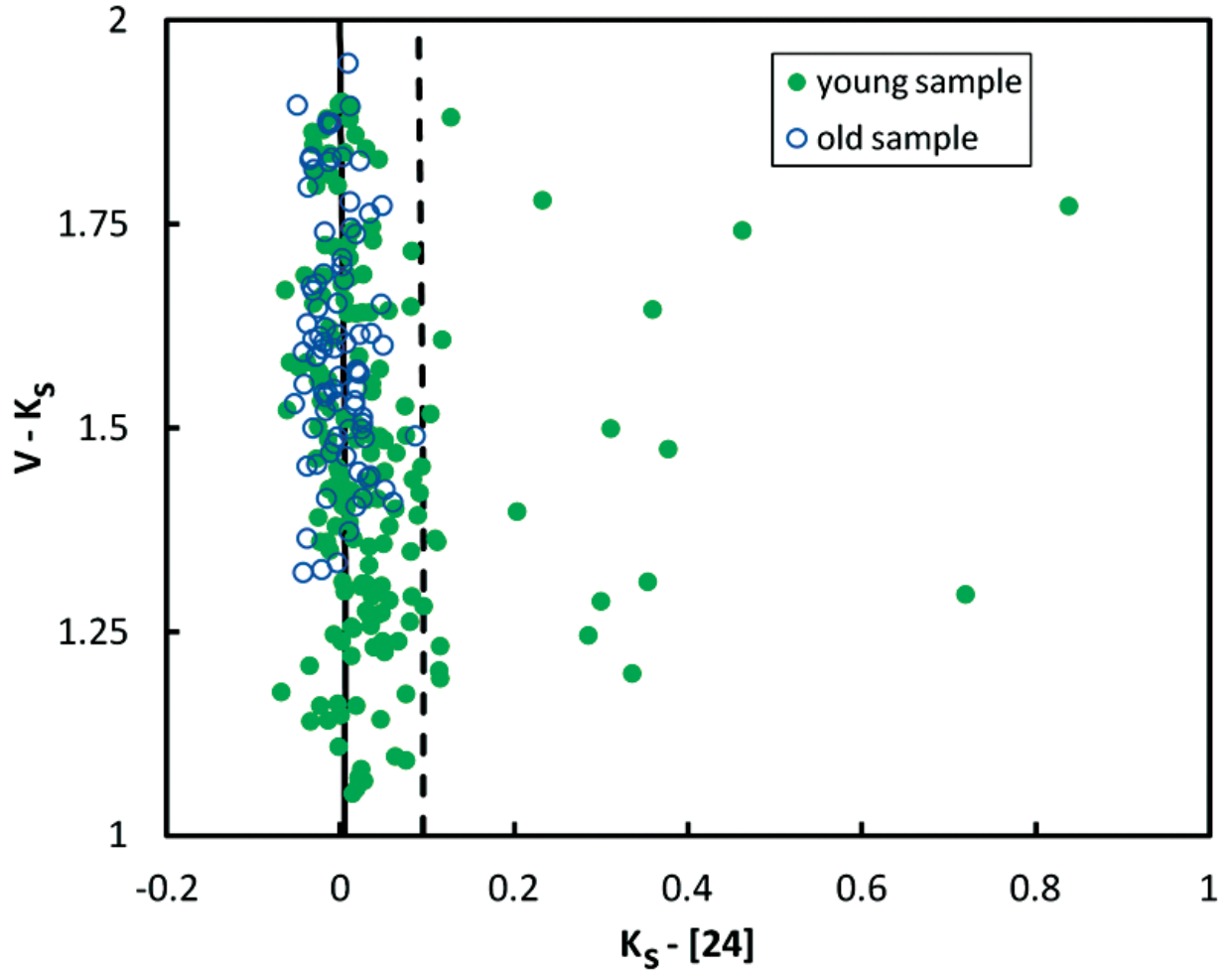


Fig. 5.— $V - K_S$ vs. $K_S - [24]$ for the final samples. The solid line represents the zero excess average (see text), while the dashed line represents the minimum for stars with excesses. Stars with extreme excesses at $24 \mu\text{m}$ are not shown.

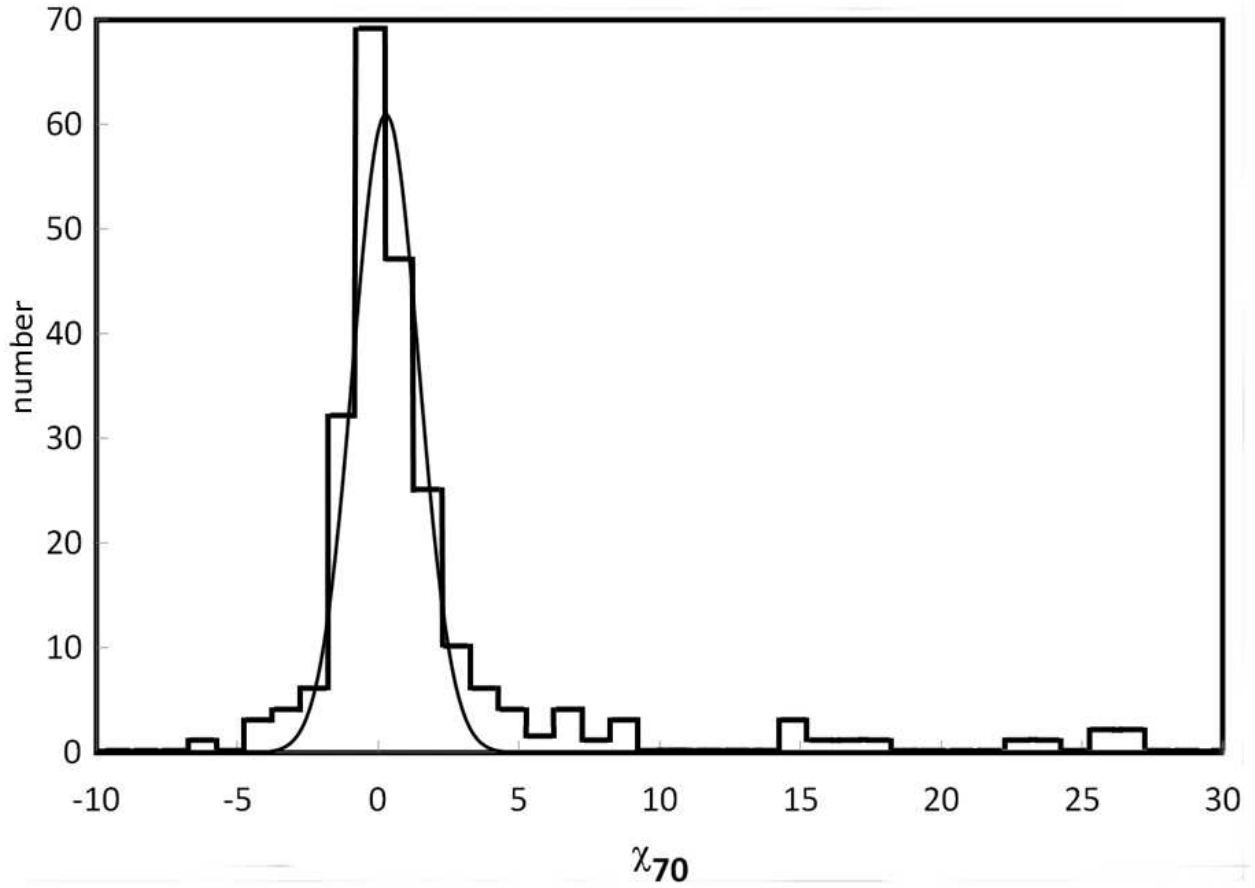


Fig. 6.— Histogram showing the distribution of χ_{70} for our sample. Some extreme values are not shown. The Gaussian fit to the distribution indicates the behavior of the purely photospheric detections.

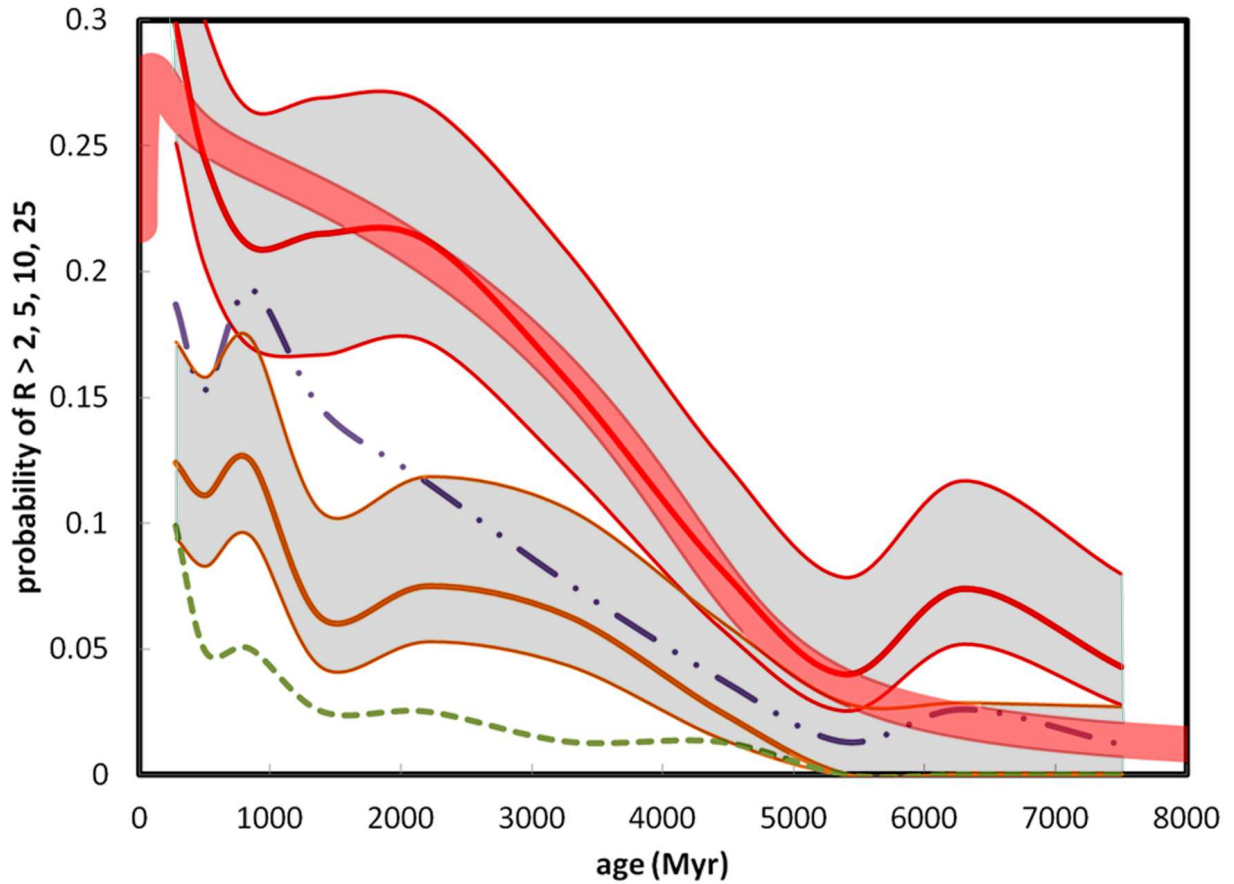


Fig. 7.— Trend of far infrared excesses with age (as measured by R , the ratio of the measured far infrared flux density to the expected value for the stellar photosphere). The trends are smoothed with an eighty-star running average; for $R = 2$ (red line) and $R = 10$ (orange), they are shown with grey zones indicating the 1σ uncertainties. The trends for $R = 5$ (blue dot-dashed line) and $R = 25$ (green dashed line) are also shown. A theoretical model for the $R = 2$ case (discussed in the text) is shown as the broad red line.